

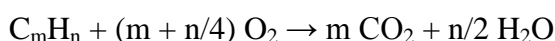
# Gold and silver catalysts for abatement of environmentally harmful materials: modelling the structure dependency

## SCIENTIFIC REPORT OF NNF2 85631 PROJECT

### 1. Introduction

The catalysis has traditionally been associated with the chemical and refinery industry and the production of chemicals with increased yields, decreased waste and decreased volumes of pollutants. However, it is only since the 1970's that catalysis has become familiar to the general public, mainly because of developments in environmental protection being the well-known and widely used catalytic converter for vehicles. To date, almost all vehicles are equipped with internal combustion engines with either spark-ignited or compression-ignited devices.

The energy is released by flame combustion of fossil fuels in the reaction with oxygen present in air:



Carbon dioxide and water are the main products of this reaction but incomplete combustion of the fuel causes the emission of other, more harmful, products (including hydrocarbons, and carbon monoxide). Most fossil fuels have some amount of sulphur-containing and nitrogen-containing constituents as well, which results in the production of sulphur oxide and nitrogen oxide emissions. The  $NO_x$  is also formed due to the very high temperatures in the combustion process by direct reaction between nitrogen and oxygen.

Carbon monoxide is a colourless and odourless gas, and is slightly lighter than air. CO is toxic and harmful to human beings and animals. On average, an exposure at 50 ppm or greater is dangerous to human health. Levels above 300 ppm for more than 1-2 h can lead to death, and exposure to 800 ppm (0.08%) can be fatal after an hour. Nitrogen oxides ( $NO_x$ ) are also highly poisonous and present a major environmental problem such as acid rain and smog.

One of the best technological solutions in reducing engine-out emissions was the invention of the three-way catalyst (TWC). Since 1993, European Standards and Directive 94/12/EEC on ambient air quality require all new cars registered in the EU to be fitted with catalytic converters containing Pt, Pd and Rh, the elements of the platinum group (PGEs). The TWC can reduce the three main contaminants, namely CO, HC (hydrocarbons) and  $NO_x$ , to below the legislated level. The Pt and Pd are used to oxidize CO and HC, while Rh for reducing  $NO_x$ .

The present (NNF2 85631) and the previous (NNF 78837) projects are aimed at developing a novel family of catalysts, based on gold and silver, to replace the more expensive and environmentally harmful platinum, palladium and rhodium metals. Such precious metals are the most promising alternative candidates as active catalysts for automotive exhaust gas pollutants abatement. According to our earlier results the manganese oxide and cobalt oxide can be a good component of the catalyst for the basic reactions for automotive pollution control. [Viacheslav Iablokov, Krisztina Frey<sup>#</sup>, Olga Geszti and Norbert Kruse: High catalytic activity in CO oxidation over unsupported  $MnO_x$  nanocrystal *Catalysis Letters*, 134, 210-216, 2010]

In addition to the CO oxidation, the preferential CO oxidation in hydrogen was also studied, although it was not foreseen in the proposal. The development of novel power generation systems, such as fuel cells, has increased the interest towards hydrogen as energy carrier during the last years. In particular, PEM fuel cells appeared the most suitable technology for distributed power generation, also due to their very low operating temperature (about 80°C). On the other hand, it is well known the very low tolerance of the Pt-based anodes to CO poisoning. Among different processes proposed for  $H_2$  purification from carbon monoxide, CO preferential oxidation (CO-PROX) is very promising due to its low cost, effectiveness and the possibility to reduce CO content down to very low level (less than 100 ppm) without a large  $H_2$  consumption. According to the literature our catalysts were promising in this reaction.

## 2. MnO<sub>x</sub> samples

### 2.1 Formation and catalytic activity in CO oxidation

Non-stoichiometric MnO<sub>x</sub> and MnO<sub>y</sub> with high CO oxidation activity at room temperature were prepared by temperature-programmed oxidation of MnC<sub>2</sub>O<sub>4</sub>·3H<sub>2</sub>O and MnC<sub>2</sub>O<sub>4</sub>·2H<sub>2</sub>O, respectively.

Catalysts were prepared in a two-step procedure. First, Mn-oxalate was precipitated from an aqueous solution of oxalic acid by adding Mn(NO<sub>3</sub>)<sub>2</sub>·4H<sub>2</sub>O at room temperature while stirring continuously and adjusting the pH value to between 6 and 9 using ammonia. The precipitation times were 40 minutes and 24 hours for producing MnC<sub>2</sub>O<sub>4</sub>·3H<sub>2</sub>O and MnC<sub>2</sub>O<sub>4</sub>·2H<sub>2</sub>O, respectively, after filtration, washing and drying overnight at 343K. The as-prepared Mn-oxalates were subsequently transformed into manganese oxides using temperature-programmed oxidation (TPO). The decomposition/oxidation performed in a mixture of 10% oxygen in Ar while heating from room temperature to 633 K at a rate of 3 K·min<sup>-1</sup>. Samples were kept for 20 min at the maximum temperature before cooling them to ambient temperature in pure Ar using the same gas flow rate. In addition, for comparison purposes, a “calcined MnO<sub>x</sub>” sample was prepared by heating MnC<sub>2</sub>O<sub>4</sub>·3H<sub>2</sub>O in a crucible under the same TP conditions but using air rather than O<sub>2</sub>/Ar.

(High resolution) Transmission Electron Microscopy ((HR)TEM), X-ray diffraction (XRD), X-ray photoelectron spectroscopy (XPS), RAMAN microscopy, TPO, TPD and X-ray absorption near-edge spectroscopy (XANES) were used to characterize MnO<sub>x</sub> and, for comparison purposes, standard stoichiometric MnO, Mn<sub>2</sub>O<sub>3</sub>, Mn<sub>3</sub>O<sub>4</sub> and MnO<sub>2</sub>.

The HRTEM micrographs along with the XRD and RAMAN spectra of the obtained manganese oxalate dihydrate and manganese oxalate trihydrate were used in order to determine the phase of manganese oxalate. The MnC<sub>2</sub>O<sub>4</sub>·2H<sub>2</sub>O sample consists of rods about 500 nm in diameter and 3–4 μm in length together with numerous smaller broken crystals. These microrods are smaller than those in the MnC<sub>2</sub>O<sub>4</sub>·3H<sub>2</sub>O sample which are typically about 1 μm in diameter and at least 20–30 μm in length. XRD and RAMAN patterns corresponding to the TEM micrographs confirm the occurrence of crystalline MnC<sub>2</sub>O<sub>4</sub>·2H<sub>2</sub>O and MnC<sub>2</sub>O<sub>4</sub>·3H<sub>2</sub>O, respectively.

Manganese oxalate thermal decomposition may lead to various forms of stoichiometric and non-stoichiometric oxides. In fact, the final product composition is largely influenced by the specific experimental conditions such as the heating mode (temperature-programmed vs stationary), gas phase composition, dynamic flow or static batch and others. Most of the oxalate decomposition experiments were done in the TPO mode. Typical TPO profiles were presented in our earlier paper (Cat. Lett.).

After thermal decomposition the MnO<sub>x</sub> and MnO<sub>y</sub> samples were tested in CO oxidation reaction at room temperature. Both oxides provide high specific surface areas (525 m<sup>2</sup>g<sup>-1</sup> and 385 m<sup>2</sup>g<sup>-1</sup>, respectively) and identical reaction rates of 10<sup>-2</sup> molecules nm<sup>-2</sup>s<sup>-1</sup> (0.017 μmol<sub>CO</sub>·m<sup>-2</sup>·s<sup>-1</sup>) at 298 K. MnO<sub>x</sub> which was prepared by oxidation of MnC<sub>2</sub>O<sub>4</sub>·3H<sub>2</sub>O precursor demonstrated higher activity than MnO<sub>y</sub> (MnC<sub>2</sub>O<sub>4</sub>·2H<sub>2</sub>O precursor, respectively) if expressed in terms of μmol<sub>CO</sub> g<sup>-1</sup> s<sup>-1</sup>. Therefore, it can be concluded that the “spinodal” transformation of Mn-oxalate precursors with different amounts of crystallisation water does not produce materials with different catalytic properties. The structural site requirements responsible for the catalytic CO oxidation are identical for both MnO<sub>y</sub> and MnO<sub>x</sub>. This indicates that geometrical “defect” structures at the surface of these oxides are less important for the surface reactivity than Mn-O binding energies. The respective conversion curves for the different manganese oxides are shown in Figure 2.1.

Despite the relatively large amount of oxygen used in most of the literature studies, MnO<sub>x</sub> prepared via oxalate decomposition exhibits superior catalytic activity. There seems to be no doubt that the high BET specific surface area (525 m<sup>2</sup> g<sup>-1</sup>) of the sample plays an important role in explaining this activity figure. As a second factor the relatively large amount of oxygen in MnO<sub>x</sub> (x = 1.61...1.67) must be taken into consideration. This is another manifestation of the frequently observed phenomenon that non-stoichiometric oxides with excess surface oxygen are more active than stoichiometric ones.

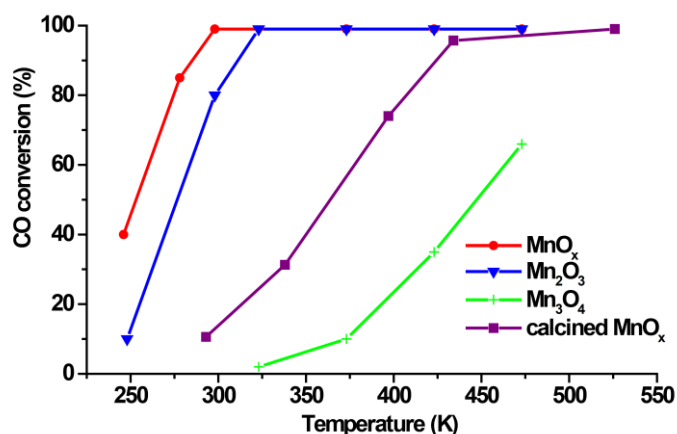


**Figure 2.1** Conversion vs. temperature for CO oxidation (2% O<sub>2</sub> + 2% O<sub>2</sub>, Ar as balance) over MnO<sub>x</sub>, Mn<sub>2</sub>O<sub>3</sub>, calcined MnO<sub>x</sub> and Mn<sub>3</sub>O<sub>4</sub> (140 mg)

For manganese oxides, prepared by oxalate route applying different decomposition/oxidation conditions the following trend of CO oxidation activity (at room temperature) were found: Mn<sub>3</sub>O<sub>4</sub> < MnO<sub>y</sub> < Mn<sub>2</sub>O<sub>3</sub> < MnO<sub>x</sub>.

The conversion data for “calcined MnO<sub>x</sub>” was plotted to demonstrate that prolonged heating at 633 K causes structural and, possibly, chemical changes of MnO<sub>x</sub>. The fast removal of crystallization water during TPO leads to the formation of MnO<sub>x</sub>, while quasi-static conditions as put into effect by using air during heat treatment in a deep crucible produces “calcined” MnO<sub>x</sub> whose catalytic activity in the CO oxidation is much lower than that of MnO<sub>x</sub> and is between Mn<sub>2</sub>O<sub>3</sub> and Mn<sub>3</sub>O<sub>4</sub>.

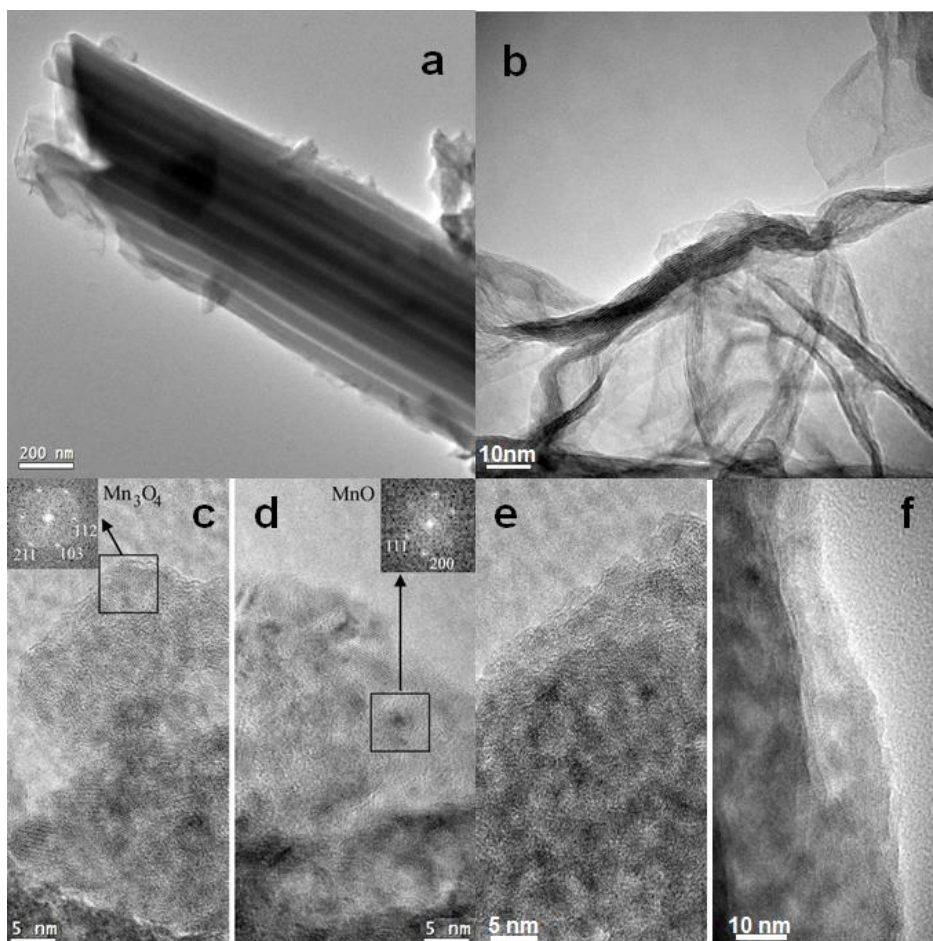
## 2.2 Structure of the highly active MnO<sub>x</sub> catalyst

We characterised only the most active MnO<sub>x</sub> catalyst.

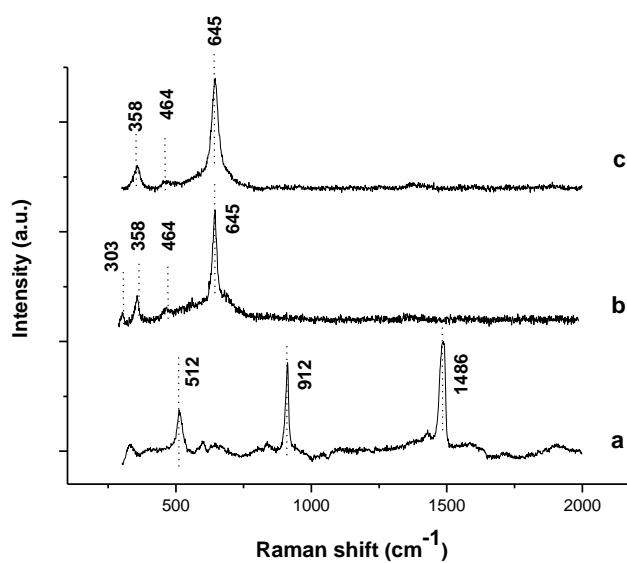
TEM investigations indicate that a “spinodal” decomposition of oxalate microrods to micro/nanorods takes place during oxidation under TPO conditions so as to produce MnO<sub>x</sub> with a particularly high BET specific surface area of 525 m<sup>2</sup> g<sup>-1</sup>. On MnO<sub>x</sub> sample various morphologies are observed and include rods, flakes and “debris” (Fig. 2.2 a and b). Flakes had a tendency to exfoliate during the CO oxidation and to create petal-shaped nanosheets around microrods. Eventually nanosized objects with sizes below 3 nm became visible in HRTEM. TEM and HRTEM both revealed a strong sensitivity to the electron beam and eventually resulted in Mn<sub>3</sub>O<sub>4</sub> and MnO nanoparticles (see Fig 2.2 c, d, e, f).

Fig. 2.3 shows the typical Raman spectrum of (a) Mn-oxalate, (b) MnO<sub>x</sub> after TPO decomposition and (c) MnO<sub>x</sub> after CO oxidation. The Fig. 2.3 a is a typical Raman spectra of Mn(C<sub>2</sub>O<sub>4</sub>) \* 3H<sub>2</sub>O, where the strongest peaks are at 1486 cm<sup>-1</sup>, 912 cm<sup>-1</sup> and 512 cm<sup>-1</sup>. The spectroscopic information and proposed assignments for manganese-oxalate in the spectral range between 2000 cm<sup>-1</sup> and 300 cm<sup>-1</sup> are shown in the Table 2.1. The (b) and (c) Raman signals in the Fig 2.3 consists of a very strong peak at 645 cm<sup>-1</sup> two smaller peaks at about 358 cm<sup>-1</sup> and 303 cm<sup>-1</sup>. They are in well agreement with the literature values for hausmannite Mn<sub>3</sub>O<sub>4</sub>, but they are broadened and down-shifted by about 15 cm<sup>-1</sup>. This down-shift is due to the particle size effect. The Raman result agreed well with the (HR)TEM results.

XANES and XPS are element-specific techniques and allow the chemical state of elements to be determined from the energy shifts of the absorption edge, as in XANES, or from the photoelectron lines, as in XPS. In particular, a more oxidative chemical environment of a given atom results in the shift of both the XANES absorption edge and the XPS binding energy of emitted electrons towards higher energies.



**Figure 2.2** Conventional and High Resolution TEM micrographs of manganese oxide after TPO activation: (a) a rod, (b) a flake on the surface of a manganese oxide rod after CO oxidation at room temperature, (c) tetragonal  $Mn_3O_4$ , (d) f.c.c.  $MnO$  phase. The Insets in (c) and (d) represent FFT-s of the areas marked by the rectangles. (e) HRTEM image taken in the first run and (f) after few minutes exposure to electron beam.



**Figure 2.3** Raman spectra of (a) Mn-oxalate, (b)  $MnO_x$  after TPO decomposition and (c)  $MnO_x$  after CO oxidation

**Table 2.1** Wavenumbers (in  $\text{cm}^{-1}$ ) and assignments of the Raman spectra of the manganese(II) oxalate  $\cdot 3\text{H}_2\text{O}$  in the spectral range between 2000 and  $300\text{ cm}^{-1}$

Raman ( $\text{cm}^{-1}$ )	Assignment
1578 w	$\nu(\text{C-O})$
1486 s	$\nu(\text{C-O})$
912 s	$\nu(\text{C-C})$
512 s	$\nu(\text{Mn-O})$
s, strong; w, weak	

Figure 2.4 shows the Mn K-edge micro-XANES spectra for various standard samples with different Mn oxidation states along with the spectrum from selected microscopic grains of  $\text{MnO}_x$ . The absorption edge in the  $\text{MnO}_x$  spectrum is seen to be located in between that of the  $\text{MnOOH}$  and  $\text{MnO}_2$  standards, indicating the Mn oxidation state in  $\text{MnO}_x$  to be between 3 and 4. The average Mn oxidation state in the  $\text{MnO}_x$  samples derived from the calibration curve is found to be  $3.4 \pm 0.1$ , which agrees well with the results of the quantitative evaluation of former TPO data. As compared to XANES which is a bulk analysis technique, XPS provides information on metal oxidation states in layers at or close to the surface.

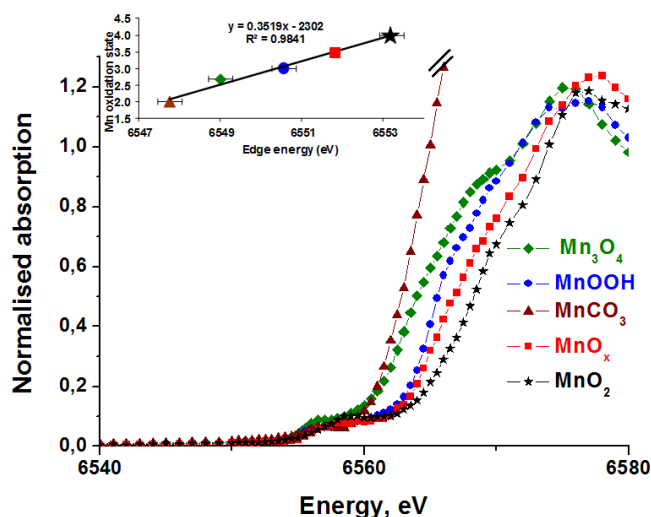


**Figure 2.4** Mn-K edge micro-XANES spectra of microscopic grains of standards and  $\text{MnO}_x$  with an inset of calibration line for Mn oxidation state determination based on the chemical shift of the absorption edge energy of standards.

Figure 2.5 presents Mn 2p, Mn 3s and O 1s core-level spectra of  $\text{Mn}_2\text{O}_3$ ,  $\text{MnO}_x$  and  $\text{MnO}_2$  plotted on a charge-corrected binding energy scale. Respective spectra for  $\text{Mn}_3\text{O}_4$  are rather similar to those of  $\text{Mn}_2\text{O}_3$  and therefore are not shown for clarity. As can be seen from Figure 5.a, the Mn 2p spectra are not too sensitive to variations in the oxidation state of manganese. The binding energy of the Mn  $2p^{3/2}$  peak in  $\text{MnO}_2$  is shifted with respect to that in  $\text{Mn}_3\text{O}_4$  and  $\text{Mn}_2\text{O}_3$  by about 0.65 eV, with practically no difference being observed between the peak positions of  $\text{MnO}_2$  and  $\text{MnO}_x$ . The Mn 3s spectra turned out to be more sensitive to the Mn oxidation state than the Mn 2p photoelectron lines. The difference in the Mn 3s peak positions in  $\text{MnO}_2$  and  $\text{Mn}_2\text{O}_3$  amounts to 0.95 eV, with the energy difference between the lines in  $\text{MnO}_x$  and  $\text{MnO}_2$  being about 0.3 eV (Figure 2.5 b). Note that both the energy position of the Mn 3s line and the multiplet splitting of the

Mn 3s photoelectron line (energy separation between two peaks) display a significant variation in the Mn oxides.

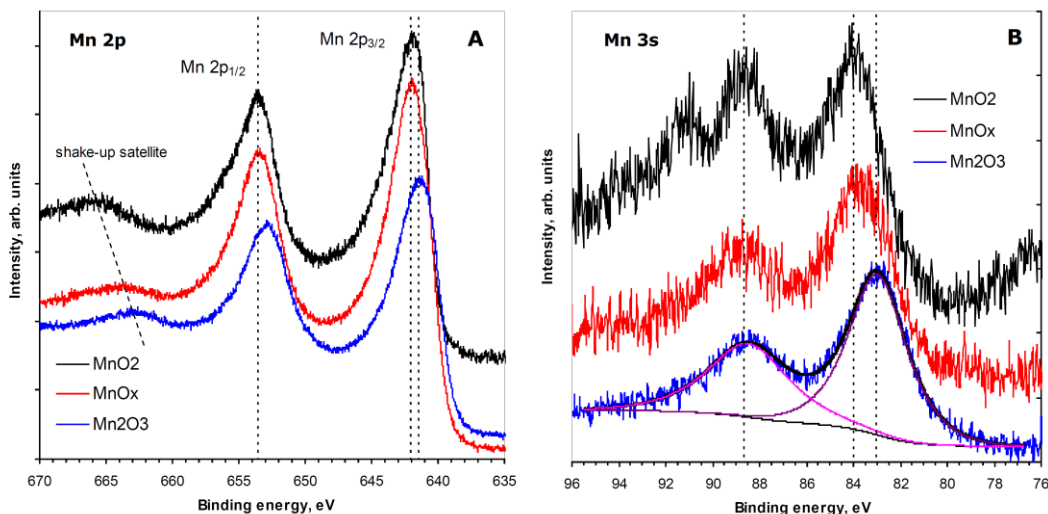


**Figure 2.5** (a) Mn 2p, (b) Mn 3s core-level XP spectra. The results of the spectra deconvolution are also shown in (b)

The magnitudes of the multiplet splitting in the studied oxides were derived from deconvolution of the Mn 3s spectra (Figure 2.5 b) and are presented in Figure 2.6. As can be seen, the energy separation between the two peaks in the Mn 3s spectrum decreases with increasing Mn oxidation state, and the multiplet splitting of the  $\text{MnO}_x$  catalyst, equal to 5.14 eV, lies between that of the  $\text{Mn}^{3+}$  and  $\text{Mn}^{4+}$  states.

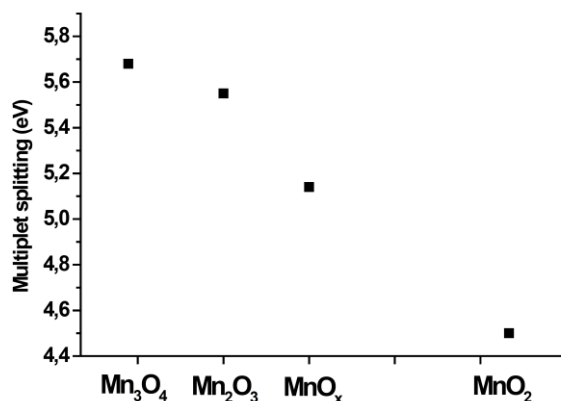


**Figure 2.6** Mn 3s multiplet splitting for oxides  $\text{Mn}_3\text{O}_4$ ,  $\text{Mn}_2\text{O}_3$ ,  $\text{MnO}_x$  and  $\text{MnO}_2$

By plotting the Mn 3s multiplet splitting versus the formal Mn valence in the oxides we evaluated the average Mn oxidation state in  $\text{MnO}_x$ . Using a linear approximation for the multiplet splitting values in the reference oxides  $\text{Mn}_3\text{O}_4$ ,  $\text{Mn}_2\text{O}_3$  and  $\text{MnO}_2$ , Mn oxidation state of 3.37 is obtained for  $\text{MnO}_x$ . This value is in very good agreement with the Mn oxidation state in  $\text{MnO}_x$  obtained from XANES bulk state analysis, and chemical titration in TPO.

CO-TPR studies were carried out in the absence of gaseous oxygen by ramping up the temperature in the presence of CO and comparing the behavior of  $\text{MnO}_x$  with that of  $\text{Mn}_2\text{O}_3$  and  $\text{Mn}_3\text{O}_4$ . The results are shown in Figure 2.7.

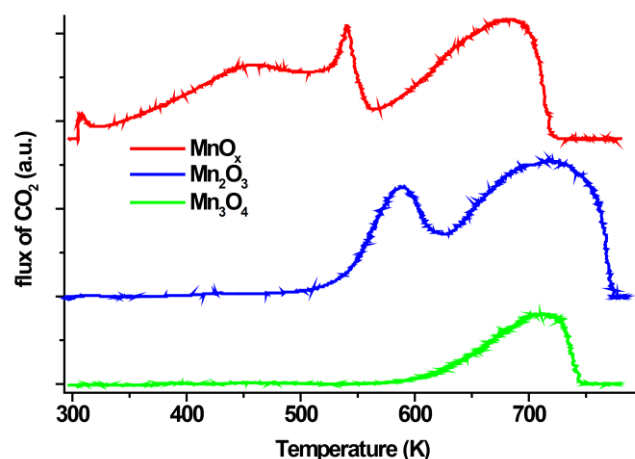


**Figure 2.7** CO-TPR profiles of manganese oxides

Obviously,  $\text{MnO}_x$  is much more reactive than the other oxides. It indicates that the active oxygen species formed during the TPO activation on the  $\text{MnO}_x$  can react with the CO even at ambient temperature. While  $\text{CO}_2$  formation starts at  $\sim 300$  K and extends over a broad range of temperatures up to  $\sim 700$  K, both  $\text{Mn}_2\text{O}_3$  and  $\text{Mn}_3\text{O}_4$  react in a limited range of temperatures much higher than 300 K. The overall behavior is in agreement with a stepwise decomposition to MnO. Obviously, mixed-valence  $\text{Mn}_3\text{O}_4$  is reduced to MnO at temperatures above 600 K, the peak maximum occurring at 713 K. The reduction profile of bulk  $\text{Mn}_2\text{O}_3$  is more complicated as two peaks with  $T_{\text{max}} = 588$  K ( $\text{Mn}_2\text{O}_3 \rightarrow \text{Mn}_3\text{O}_4$ ) and 718 K ( $\text{Mn}_3\text{O}_4 \rightarrow \text{MnO}$ ) occur. The reduction of  $\text{MnO}_x$  shows pronounced peaks at 540 K and 683 K. The stepwise decomposition of  $\text{MnO}_x$  is a nice demonstration of the ‘‘Ostwald Stufenregel’’ rule.

Surface oxygen species were characterized by temperature programmed desorption method (TPD). The TPD profile for the  $\text{MnO}_x$  sample is presented in Figure 2.8.

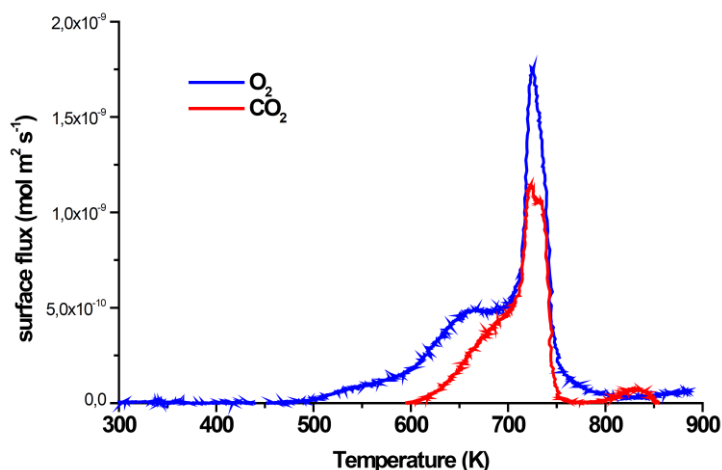


**Figure 2.8** TPD (Ar atmosphere) of  $\text{MnO}_x$

The profile shows two broad overlapped stages of desorption at 550 K and 663 K, and sharp peak at 723 K coincides with the releasing of  $\text{CO}_2$  gas. The low temperature peak centered at 550 K may be assigned to the oxygen species chemically adsorbed on the surface of  $\text{MnO}_x$  while peak around 663 K can be assigned to desorption of the surface lattice oxygen. The sharp desorption peaks of  $\text{O}_2$  and  $\text{CO}_2$  at 723 K are related of collapsing the bulk structure of  $\text{MnO}_x$  to well-crystalline bixbyite structure ( $\alpha\text{-Mn}_2\text{O}_3$ ) as it is well coincided with the TPO profile (see Figure 2.8 b). Note that the carbon source is an internal carbon, which lies in the internal structure of the oxide microrods. During transformation of the manganese oxalate into manganese oxide some oxalate bridges due to limited diffusion in a solid material may be reduced forming a jailed coke.

Subsequently, at the moment of collapsing the structure, the coke is being oxidized by available mobile lattice oxygen species.

The findings of the kinetic studies suggest that the adsorption of both molecules, CO and O<sub>2</sub>, is followed by their surface reaction via carbonate/formate-like intermediates to produce CO<sub>2</sub>. We assume a Mars-van Krevelen type mechanism where oxygen belonging to the MnO<sub>x</sub> structure takes part in the catalytic CO oxidation. However, these mobile oxygen species are not part of the bulk oxide lattice, and therefore they are able to “hop” on the surface and feed the oxygen species needed for the oxidation of previously adsorbed CO.

### 3. CoOx, MnOx and MnCoOx samples

Since the Mn-oxalate precipitation followed by temperature programmed decomposition/oxidation provided high surface area Mn-oxide of exceptional high CO oxidation activity, this preparation technique was applied for formation of Co-oxide and mixed MnCo-oxide samples. The reaction rate of oxide catalysts in oxidation reactions operating by the Mars van Krevelen mechanism varies according to a maximum curve as a function of the oxygen binding energy of the different oxides, and the Mn<sub>2</sub>O<sub>3</sub>, Co<sub>3</sub>O<sub>4</sub> and CuO was reported to be among the best performing CO oxidation catalysts. By increasing the specific surface area and modification and tuning of the lattice oxygen binding energy the catalytic activity can be increased. In total oxidation reactions these oxides are demonstrated to be also active partners in cooperation with Au nanoparticles, and expected to be active with Ag and bimetallic AuAg nanoparticles, too, what was planned to study in the present project. However, before the investigation of the more complex MnOx, CoOx or MnCoOx supported Au, Ag and AuAg catalysts, the own structural and catalytic properties of the pure oxides seemed to be reasonable. The pure oxides without noble metal were tested in CO oxidation reaction, in selective catalytic reduction of NO by CO (NO+CO) and in preferential CO oxidation in H<sub>2</sub> (PROX). As synergetic effect of the mixed MnCo-oxide was experienced in CO oxidation and PROX reaction, while in NO+CO such synergism was not observed, we decided to study these systems in the PROX process more detailed to reveal the relation between the structural and catalytic properties.

#### 3.1 Preparation and structural characterization of the samples

Manganese oxide (MnOx), cobalt oxide (CoOx) and manganese-promoted cobalt oxide (1Mn8CoOx, 5Mn5CoOx) with Mn/Co=11/89 and 50/50 intended atomic ratio, respectively, were prepared by precipitating Mn-, Co- and MnCo-oxalate from nitrate precursors. As a reference, manganese-promoted cobalt oxide with nominal Mn/Co=11/89 were prepared by MnCo-carbonate precipitation (1Mn8CoOx-C). The oxalates and carbonates were calcined at 360°C for 20 min in 10%O<sub>2</sub>/He after heating up by 3°C/min rate, and at 350°C for 5 h in air after heating up by 10°C/min rate, respectively.

The catalysts were characterized by N<sub>2</sub> adsorption, XRD, TEM equipped with EDS, HRTEM, conventional XPS and synchrotron based in situ XPS, XAS and XANES.

Table 3.1 summarises the structural results of the samples studied. Three Mn-oxide samples (MnOx\_1-3) were prepared according to the oxalate route applied for sample designated by MnO<sub>x</sub> described above in the “MnOx samples” section. Only the TPO decomposition differed slightly, as larger amount of oxalate (1-2 g) were treated in one batch, for MnOx\_1 20%O<sub>2</sub>/He was applied in TPO, and the position of Mn-oxalate were different in the U-type reaction tube (it was located in the vertical part forming a compact bed, or in the bottom of the U-tube) causing different contact with the reactant gas. The specific surface area and even the stoichiometry of the resulting oxides were different. Unfortunately, the specific surface areas of the MnOx\_1-3 have not reached that of the highly active MnO<sub>x</sub> presented in the previous section. The largest, 104 m<sup>2</sup>/g specific surface area MnOx\_3 consisted of very small Mn<sub>3</sub>O<sub>4</sub> crystallites accompanied with significant amount of X-ray amorphous fraction. The decomposition/oxidation step of the preparation, especially providing the optimal temperature, concentration of O<sub>2</sub> and decomposition products along the catalyst bed seems

to be a very sensitive part of this preparation. The reproducibility of Co-oxide preparation was much better, the composition of the two batch of Co-oxide prepared (CoOx\_1-2) and their specific surface area was similar, except the crystallite size of the Co<sub>3</sub>O<sub>4</sub> differed somewhat. The final Mn/Co atomic ratio in the mixed MnCo-oxides prepared via oxalate route (1Mn8CoOx and 5Mn5CoOx) were much smaller, 5/95 and 12/88, than the intended Mn/Co=11/89 and 50/50 ones, respectively. The precipitation of Mn-cations in oxalate form was less efficient than that of Co in the conditions applied. In 1Mn8CoOx\_C formed via carbonate route the real Mn/Co ratio was closer to the expected one, 8/92 instead of 11/89. All three mixed oxide possessed similar specific surface area that was significantly larger than that of the monometallic oxide analogous except MnOx\_3. On Fig. 3.1 the morphology of 5Mn5Co-oxalate and 1Mn8Co-carbonate and the oxides derived from them can be compared. The precursor states were significantly different, but the two oxides had similar morphology. The X-ray diffraction patterns of the mixed oxides were almost identical with that of Co<sub>3</sub>O<sub>4</sub>. For the more precise evaluation of XRD results corundum internal reference was added in 20 wt% to several samples to determine the precise lattice parameter and to estimate the concentration of the crystalline phases in these samples.

**Table 3.1** Structural data of the catalysts

<i>Samples</i>	<i>Mn/Co (EDS)</i>	<i>Secific surface area m<sup>2</sup>/g</i>	<i>Crystallite size nm</i>	<i>Lattice parameter Å</i>	<i>Crystalline phases</i>	<i>Oxidation state of Mn</i>	<i>Oxidation state of Co</i>
MnO <sub>x</sub> (see in previous section)	-	525	1-3		Mn <sub>5</sub> O <sub>8</sub>	+3.4 (XANES)	-
MnOx_1	-	n.a.	55		Mn <sub>3</sub> O <sub>4</sub>	+3.0 (XANES)	-
MnOx_2	-	31	47		Mn <sub>2</sub> O <sub>3</sub>		-
MnOx_3	-	104	12		*Mn <sub>3</sub> O <sub>4</sub> + ≈40-50% amorphous		-
CoOx_1	-	54	58	8.084	*Co <sub>3</sub> O <sub>4</sub> + ≈10-15% amorphous	-	+2.6 (XANES)
CoOx_1 700°C/air/3h	-	n.a.	980	8.084	*Co <sub>3</sub> O <sub>4</sub> + <10% amorphous	-	
CoOx_2	-	50	29	8.084	Co <sub>3</sub> O <sub>4</sub>	-	
CoOx_2 700°C/2h/air	-	10				-	
1Mn8CoOx	5/95	70	34		Mn <sub>k</sub> Co <sub>3-k</sub> O <sub>4</sub>	+3.6 (XANES)	+2.6 (XANES)
1Mn8CoOx 700°C/2h/air		30					
5Mn5CoOx	12/88	79	20	8.11	*Mn <sub>m</sub> Co <sub>3-m</sub> O <sub>4</sub> + ≈25-35% amorphous		
5Mn5CoOx 700°C/air/3h		20	29	8.15	*Mn <sub>n</sub> Co <sub>3-n</sub> O <sub>4</sub> + <10% amorphous		
1Mn8CoOx_C	8/92	76	32		Mn <sub>1</sub> Co <sub>3-1</sub> O <sub>4</sub>		+2.5 (XANES)
* XRD measurements were performed with corundum internal reference							

Characteristic diffractograms are shown on Fig. 3.2, where clear shift of the  $\text{Co}_3\text{O}_4$  reflections can be seen in the  $5\text{Mn}5\text{CoOx}$ , and further shift after its high temperature treatment ( $700^\circ\text{C}/3\text{h}/\text{air}$ ). The increase of the lattice parameter must have been caused by the substitution of Co by Mn ions in the  $\text{Co}_3\text{O}_4$  lattice. After high temperature treatment, the extent of Mn substitution increased, while the original, about 30% amorphous phase content decreased to about its estimation limit. It means that Mn content must have been higher in the amorphous part of the as prepared sample. Further important effect of the high temperature treatment was the sintering of the sample, resulting in larger crystallite size and smaller surface area also in case of  $1\text{Mn}8\text{CoOx}$ . The same high temperature treatment of  $\text{CoOx}$  caused more dramatic sintering and crystallization of the small, about 10-15% amorphous part.

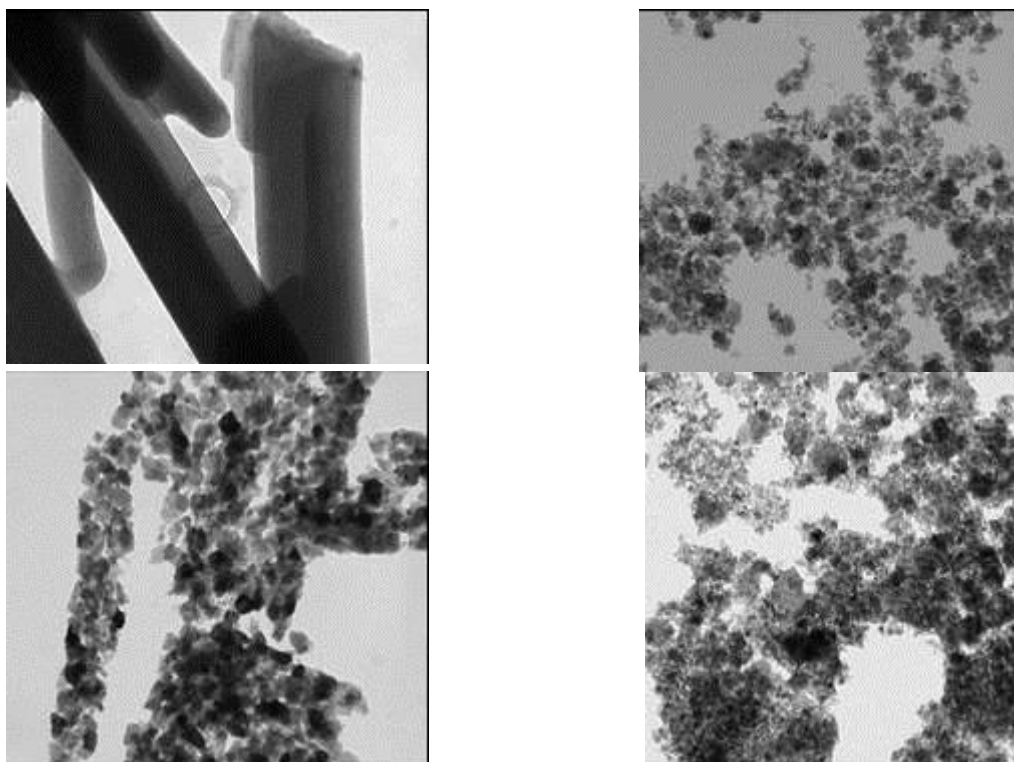


**Figure 3.1** TEM micrographs of  $5\text{Mn}5\text{Co}$ -oxalate and  $1\text{Mn}8\text{Co}$ -carbonate (upper pictures) and the mixed oxides derived from them (lower pictures)

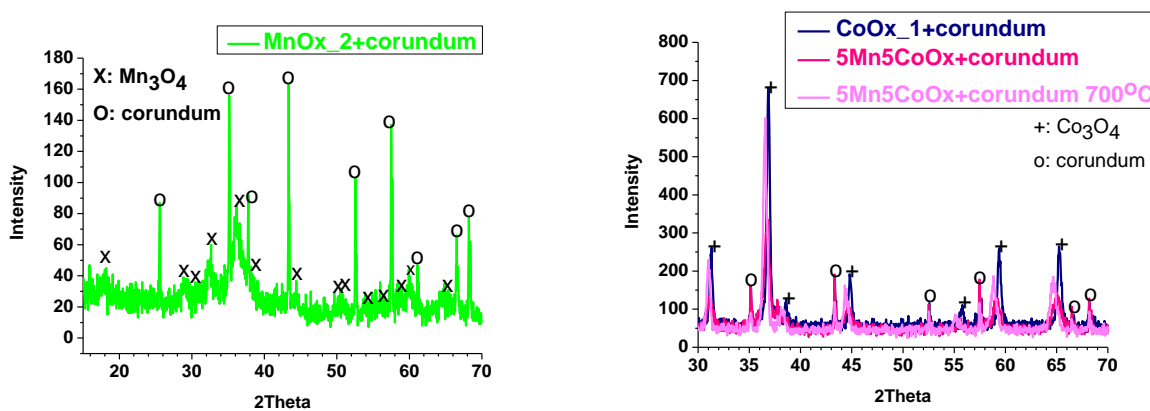


**Figure 3.2** X-ray diffractograms of  $\text{MnOx}_3$ ,  $\text{CoOx}_1$ ,  $5\text{Mn}5\text{CoOx}$  in as prepared state and  $5\text{Mn}5\text{CoOx}$  after  $700^\circ\text{C}/3\text{h}/\text{air}$  treatment. Corundum as internal standard was added to the samples in 20 wt%.

The homogeneity of the structure was probed in the 5Mn5CoOx by HRTEM measurements in comparison with CoOx\_2 using Au nanoparticles as internal standard. Three typical micrographs and the distribution of lattice parameters measured at different spots in the mixed oxide can be seen on Fig. 3.3. The error of the lattice parameter measurement was about  $\pm 0.1$  Å, and most of the crystallites measured had value in between those of Co<sub>3</sub>O<sub>4</sub> and MnCo<sub>2</sub>O<sub>4</sub>. No other type of periodicity was perceived. We might suppose that there was a distribution of the extent of the Mn substitution in the different crystallites. However, we cannot say anything about the positions of the Mn substitution. The measurement of the oxidation state of Mn and Co can give further structural information relevant concerning the catalytic properties.

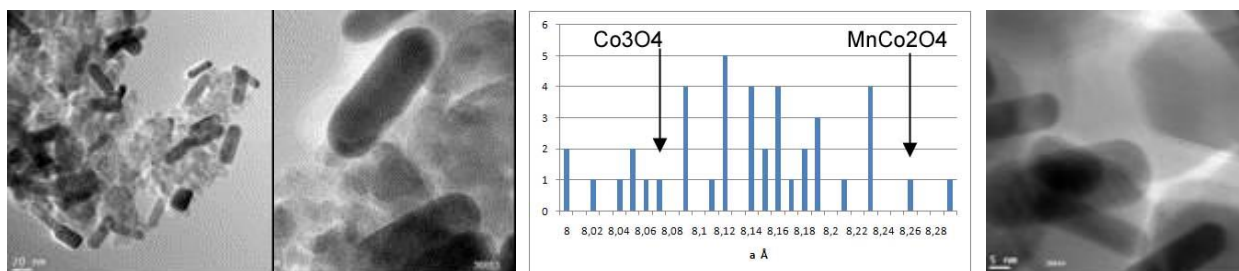


**Figure 3.3** HRTEM micrographs of 5Mn5CoOx (on the left), histogram of lattice parameter measured on 5Mn5CoOx at different spots, and HRTEM micrograph of 5Mn5CoOx after 700°C/3h/air treatment (on the right). Au nanorods were added onto the reverse side of the grid as internal reference.

X-ray absorption measurements, XANES and XAS can identify the chemical environment of the investigated cationic center, thus a certain chemical state does not necessarily mean a long-range ordered phase as XRD indicate. On Fig. 3.4 the Co L-edge X-ray absorption near edge spectra of the oxalate derived CoOx\_1 and 1Mn8CoOx and the carbonate derived 1Mn8CoOx\_C samples are presented along with Co<sup>2+</sup> and Co<sup>3+</sup> containing reference materials. The spectra of our three Co-containing samples almost perfectly fitted with each other and were very similar to that of Co<sub>3</sub>O<sub>4</sub> reference spectrum. From this the presence of the same type of Co cationic sites in the mixed oxides as in Co<sub>3</sub>O<sub>4</sub> could be deduced. The average Co oxidation state determined was +2.6 for the oxalate derived samples and +2.5 for 1Mn8CoOx\_C. The Mn oxidation state determined from the Mn L-edge absorption spectrum of 1Mn8CoOx (not shown) was +3.6.

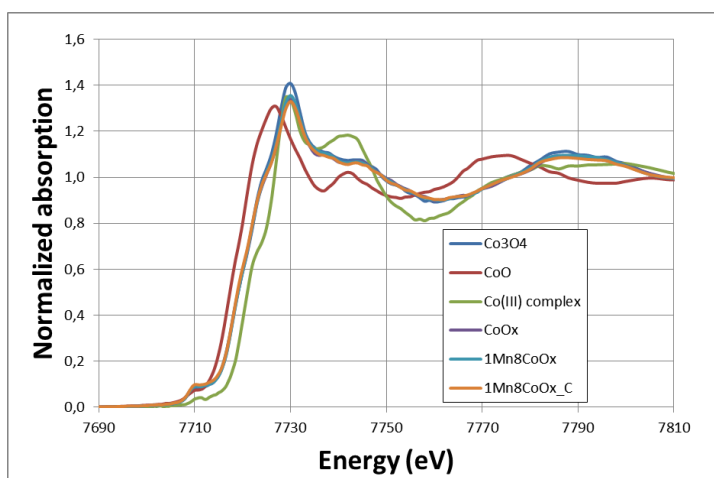


**Figure 3.4** Co L-edge XANES spectra of CoOx\_1 and 1Mn8CoOx and reference materials

Synchrotron based in situ XPS and XAS experiments of MnOx\_2, CoOx\_1 and 1Mn8CoOx have been performed under various environments modelling the different pretreatments and PROX

and CO oxidation reactions according to the following typical protocol. Spectra were recorded in steps 1, 2, 3, 5, 7 after 30 minutes.

1. 2 ml/min O<sub>2</sub>/0.2mbar (spectra denoted by „O<sub>2</sub> as received”)
2. O<sub>2</sub>/250°C (spectra denoted by „O<sub>2</sub>”)
3. 20 ml/min H<sub>2</sub>:CO:O<sub>2</sub>/18:1:1/1mbar/140°C (spectra denoted by „PROX”)
4. O<sub>2</sub>/250°C/30’
5. 4ml/min CO:O<sub>2</sub>/1:1/0.3mbar/140°C (spectra denoted by „CO+O<sub>2</sub>”)
6. O<sub>2</sub>/250°C/30’
7. 18 ml/min H<sub>2</sub>/1mbar/140°C (spectra recorded denoted by „H<sub>2</sub>”)

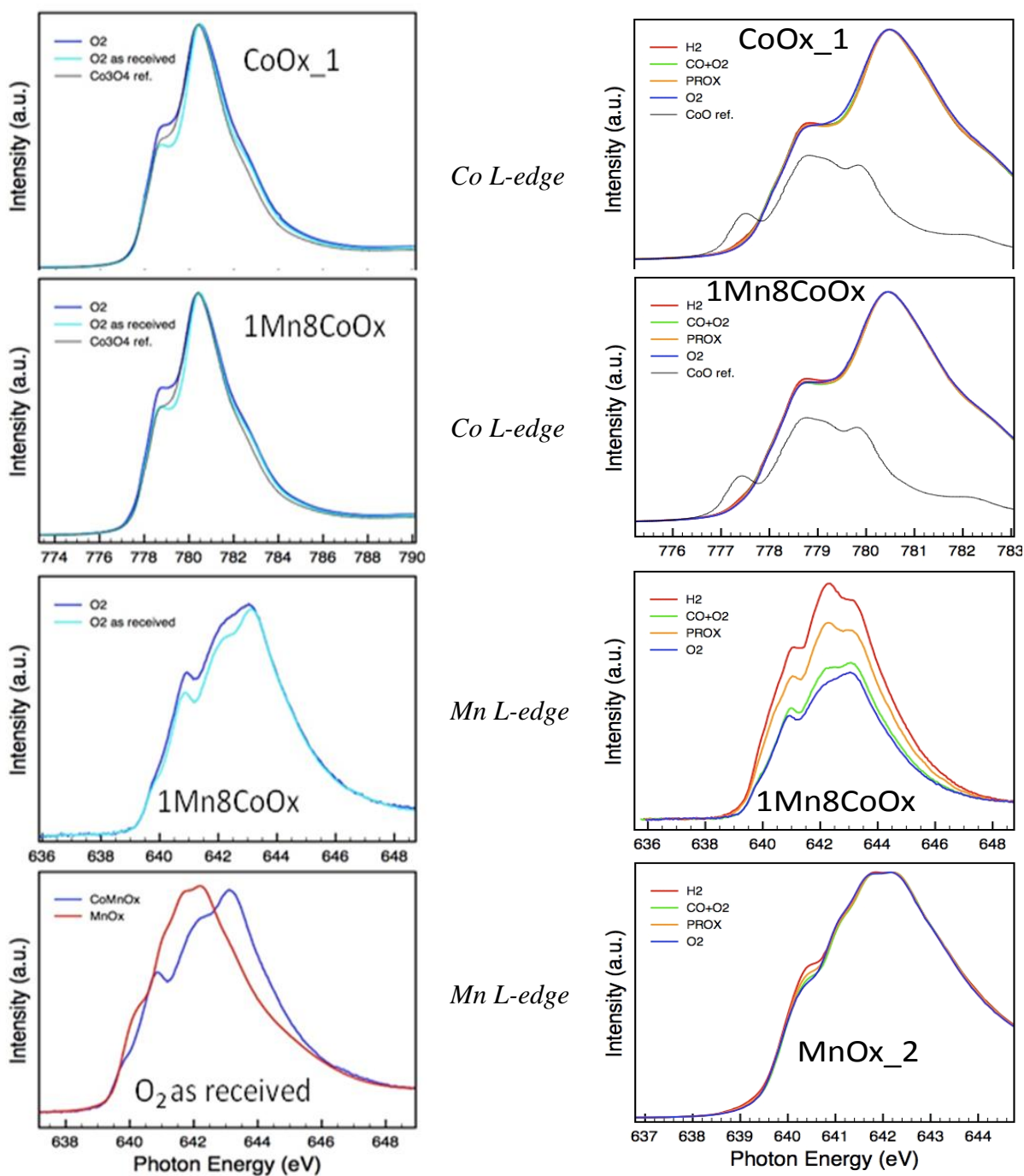


**Figure 3.5** In situ synchrotron based Co L-edge and Mn L-edge spectra of CoOx\_1, MnOx\_2 and 1Mn8CoOx at different conditions

The XAS results are presented on Fig. 3.5, the XPS results on Figs. 3.6-3.10. According to XAS results CoOx\_1 consisted of Co<sub>3</sub>O<sub>4</sub>, and Co cations in 1Mn8CoOx in as received state were also in the same state as in Co<sub>3</sub>O<sub>4</sub>, which was in agreement with XRD and XANES results. In case of both samples the first feature of Co L-edge spectrum got more intense in 250°C oxidative treatment, which may indicate a small reduction, or it was rather a temperature effect. No significant change could be discerned after any of the above listed other treatments, at the most 2% Co<sup>2+</sup> formation could be supposed in model PROX and H<sub>2</sub> treatment conditions. The Mn L-edge spectrum of MnOx\_2 was like that of Mn<sub>2</sub>O<sub>3</sub> correspondingly with XRD result. But for 1Mn8CoOx XAS showed rather Mn<sup>4+</sup> state close to +3.6 oxidation state that was estimated by XANES, and differently as suggested by XRD, namely Mn<sup>2+</sup> or Mn<sup>3+</sup> as substituted in Co<sub>3</sub>O<sub>4</sub> lattice. An explanation can be that Mn is substituted dominantly in the Co<sup>3+</sup> positions and it is in higher oxidation states in the amorphous part of the sample. In the various treatments of 1Mn8CoOx the reduction of Mn<sup>4+</sup> to Mn<sup>3+</sup> could be observed in different extent, the most in H<sub>2</sub> treatment, the least in CO oxidation. In case of MnOx\_2 in various conditions hardly any changes could be observed except appearance of very minor amount Mn<sup>2+</sup>.

To summarize the XAS spectra, MnOx was essentially Mn<sub>2</sub>O<sub>3</sub> and only very little reduction was shown to occur even in sole H<sub>2</sub>. Both Co containing samples showed Co environment of Co<sup>2+</sup> and Co<sup>3+</sup>, representative of Co<sub>3</sub>O<sub>4</sub>. Reduction under reaction condition or in H<sub>2</sub> was at the border of detection limit. Interestingly, the Co-oxide matrix seemed to stabilize Mn in +4 oxidation state, which however readily underwent partial reduction under reaction. Reduction degree was highest in H<sub>2</sub> and decreased in the following order: H<sub>2</sub>>PROX>CO+O<sub>2</sub>>O<sub>2</sub>.

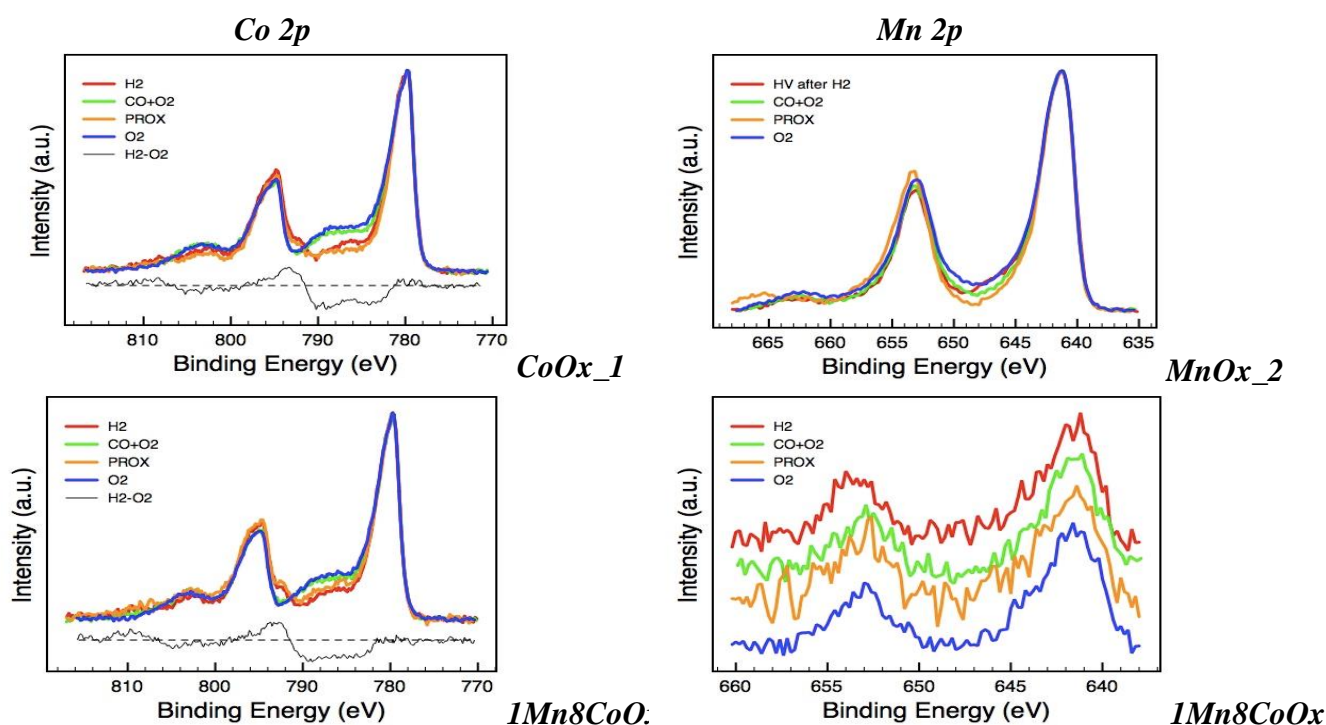


**Figure 3.6** In situ synchrotron based Co2p spectra of CoOx\_1 and 1Mn8CoOx. Spectra are shown after Shirley background subtraction.

**Figure 3.7** In situ synchrotron based Mn2p spectra of MnOx\_2 and 1Mn8CoOx. Spectra are shown after Shirley background subtraction.

XPS spectra were recorded by various excitation energies providing photoelectrons of four different kinetic energies (KE) and detection depth. The ones presented on Figs. 3.6-3.10 are the most surface sensitive spectra recorded with 200eV KE. The binding energy and the shape of the Co 2p spectra of CoOx\_1 and 1Mn8CoOx (Fig. 3.6) are characteristic of Co<sub>3</sub>O<sub>4</sub>. Note however that on the high BE side of the main doublet, satellite structure is visible, which got smaller in H<sub>2</sub> and in

PROX. The existence of satellites is characteristic of charge transfer events in the valence band. According to literature of CoO (which has even stronger satellite, though at smaller BE shift), the main line is due to  $3d^8L$  (8 Co 3d electrons with 1 hole in the O2p; that is, a charge transfer between Co3d and O2p) and the satellite is due to  $3d^7$  final state. Analogous explanation is expected here for  $Co_3O_4$ . The small peaks at approx. +13eV from the main lines in PROX and in  $H_2$  are due to inelastic scattering of the photoelectrons on  $H_2$ , thus these are not relevant for us. To identify the “chemical” origin of the modulation of the satellite intensity and to correlate this with the lack of red-ox chemistry of Co centers seen in XAS is ongoing. (The modulation of the satellite intensity is one of the most interesting aspects of these experiments.)

On Fig. 3.7 there is not much difference in the Mn2p of MnOx sample in various atmospheres (in line with the highly constant Mn L-edge), and the BE is also similar to that observed for  $Mn_2O_3$ . Note that some satellite modulation is also suggested here. Since the quality of Mn 2p in  $1Mn8CoOx$  due to the low concentration was so poor, these cannot be reliably discussed.

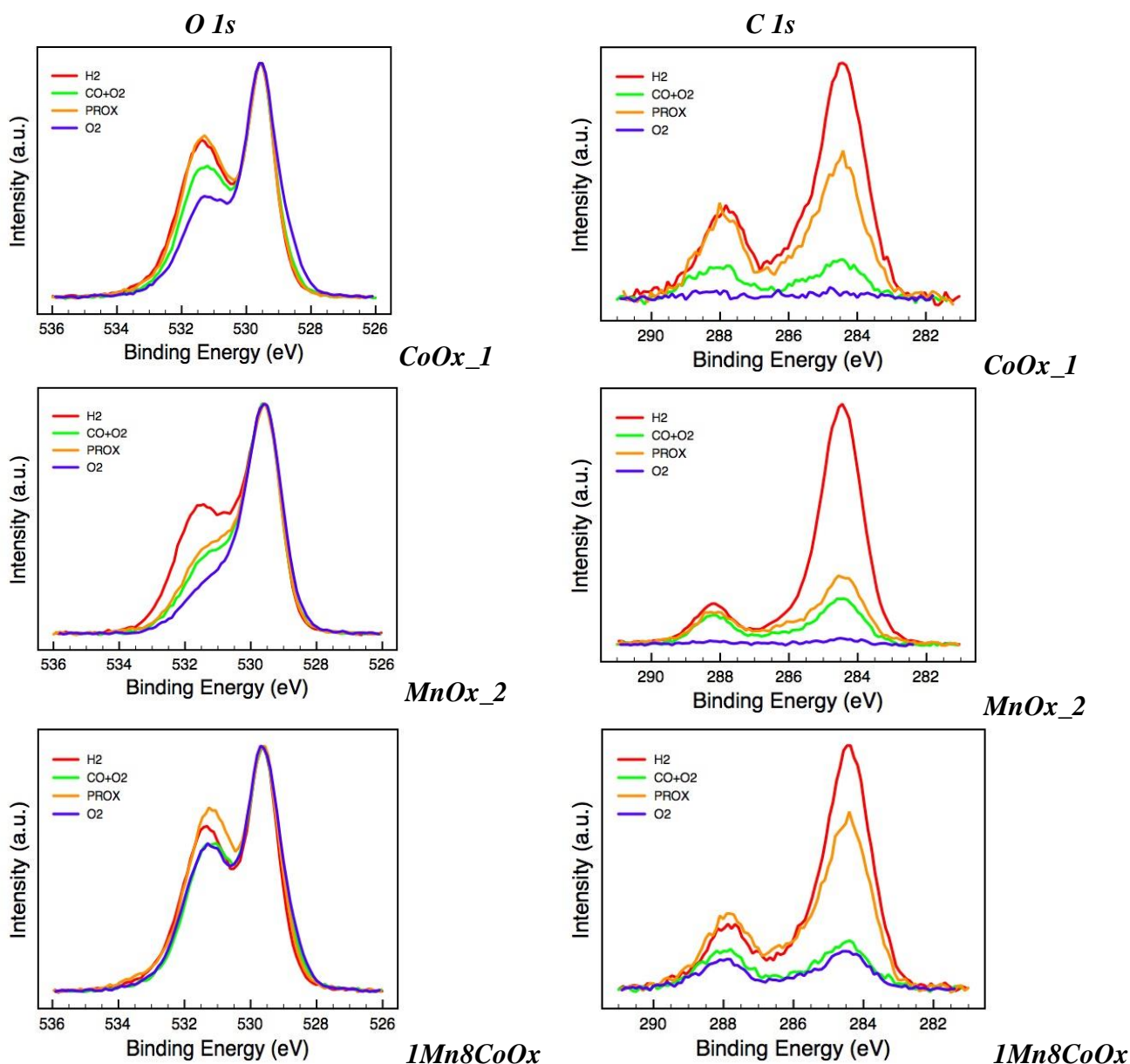


**Figure 3.8** In situ synchrotron based O1s spectra of the samples recorded in different conditions.

**Figure 3.9** In situ synchrotron based C1s spectra of the samples. Spectra within one sample are normalized to the same metal intensity.

O1s spectra (Fig. 3.8) of 1Mn8CoOx, MnOx\_2 and CoOx\_1 indicated two main components, the low BE main line (529.6 eV) characteristic of lattice “O<sup>2-</sup>” and the component at 531.x eV responsible for OH. Mainly in oxygen, but also in CO+O<sub>2</sub>, there is a small peak around 528.7 eV, which may be related to multi-coordinated surface O sites. Additionally, adsorbed water (on the high BE side of OH) and carbonates (see C1s) are hidden under the broad high BE part of the spectrum. The most surface functionalities were detected in PROX condition. O1s spectra of MnOx displayed relatively low surface functional group density, except in H<sub>2</sub>.

All three samples at all conditions (except CoOx and MnCoOx in O<sub>2</sub> with less surface sensitive excitation) showed higher oxygen content derived from the qualitative evaluation of the XP spectra than that the stoichiometry would dictate. Although cross section issues cannot be excluded, the termination of surface with O-containing functional groups can give rise to higher O/Metal ratios. However, when only the area of bulk O1s component after spectrum decomposition is considered the O/Metal values 0.8-1 are obviously under-stoichiometric, as not only new adsorbates contribute to the removed O1s part, but also O atoms originally belonging to the lattice but by breaking up O-Co bonds these created new surface functional groups.

The low BE component in C 1s spectra (see Fig. 3.9) can be attributed to carbon deposition (impurity carbon, C, CH, graphite, etc.), whereas the high BE component can be assigned to carbonates. Note that non-oxidative conditions facilitated carbon accumulation. PROX condition enabled the build-up of significant carbonate concentration.

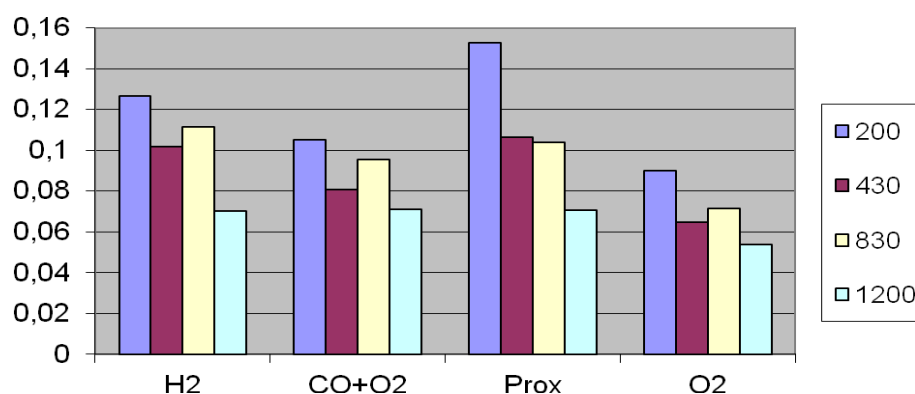


**Figure 3.10** Mn/Co ratio (calculated from Mn/Co 3p's situated next to each other in the spectrum) as a function of electron kinetic energy (200-1200 eV)

Fig 3.10 shows the variation of Mn/Co atomic ratio on the different samples between different conditions in surface layers in various depths. The surface Mn/Co atomic ratio measured were somewhat higher than the bulk Mn/Co=0,053 measured by EDS, so Mn enriched on the surface in different extent. There was more Mn in reducing conditions on the surface than in oxidizing conditions. Moreover, despite the low absolute numbers, Mn tended to be higher at lower electron kinetic energy, thus when measured with higher surface sensitivity.

Conventional XPS studies were also performed on 5Mn5CoOx and CoOx\_2 samples after consecutive treatments (i) in air flow at 360°C for 25 min, then (ii) in PROX reaction mixture flow (1%CO+1%O<sub>2</sub>+60%H<sub>2</sub>/He) at 250°C for 40 min, and (iii) again in air at 360°C for 25 min carried out in the attached atmospheric reaction chamber. The spectra of Co 2p, Mn 2p, O1s and C1s are collected in Figures 3.13-3.14. Note that the pretreatment conditions in these measurements were more severe, than in case of synchrotron based in-situ XPS studies, higher temperatures and larger pressures were used, comparable with the conditions of the PROX catalytic tests.

Both CoOx\_2 and 5Mn5CoOx showed typical Co 2p spectrum of Co<sub>3</sub>O<sub>4</sub> after the first air treatment. In the as prepared state similar spectrum (not shown) was measured, too. During PROX pretreatment the most significant changes were the increased intensity of the satellite peak at 786.5 eV in about similar extent on both the CoOx\_2 and 5Mn5CoOx, and in the mixed oxide a significant shift of peaks to higher BEs. This indicated the reduction of Co, the formation of Co<sup>2+</sup> in both samples and somewhat restructuring in the mixed oxide sample. In the repeated oxidative treatment the original state was restored.

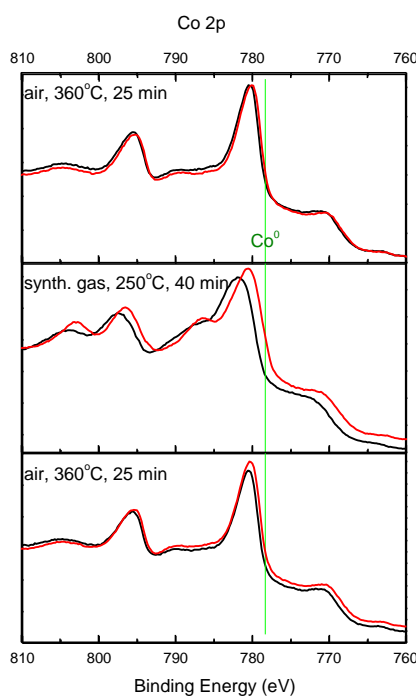


**Figure 3.11** Conventional Co 2p XPS spectra of 5Mn5CoOx (black curves) and CoOx\_2 (red curves)

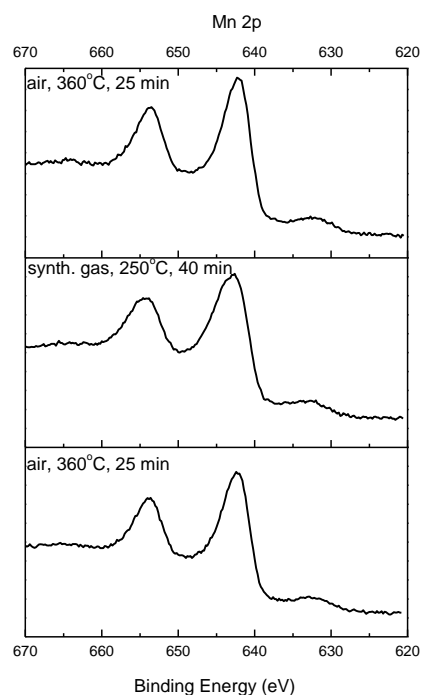


**Figure 3.12** Conventional Mn 2p XPS spectra of 5Mn5CoOx

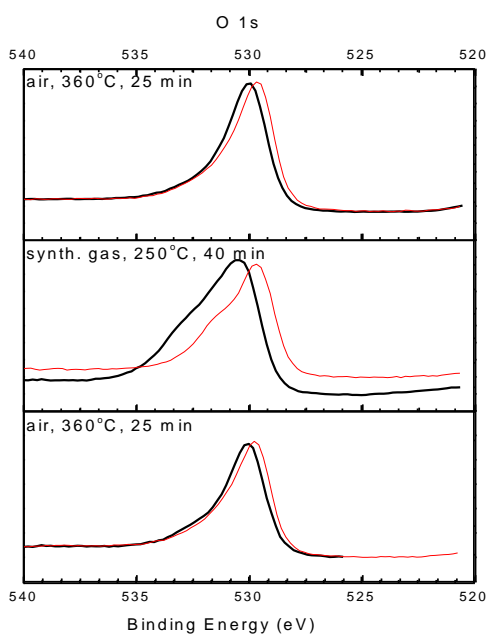


**Figure 3.13** Conventional O 1s XPS spectra of 5Mn5CoOx (black curves) and CoOx\_2 (red curves).

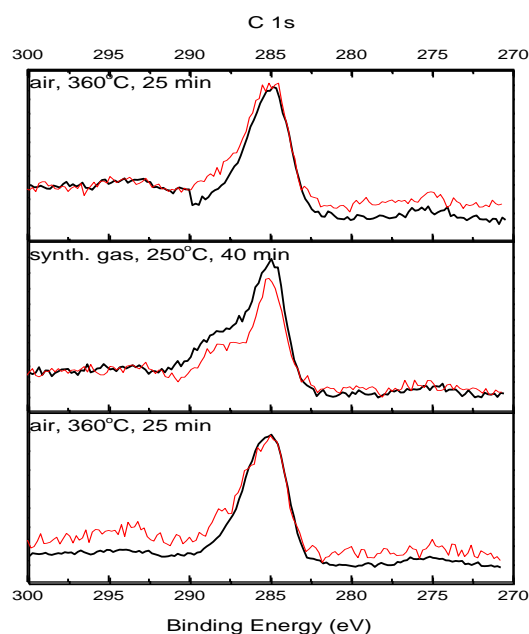


**Figure 3.14** Conventional C 1s XPS spectra of 5Mn5CoOx (black curves) and CoOx\_2 (red curves).

In case of the mixed oxide sample the Mn 2p spectrum showed some changes in the different treatment, as 0.5 eV shift to higher BE-s and minor widening of the peaks under PROX conditions. These changes were reversible, re-oxidation resulted in the formation of the original spectrum. The O 1s spectra indicated that the two samples in oxidised state were similar concerning both the shape and position. Beside the main peak belonging to the lattice oxygen the higher BE shoulder showed

the presence of some hydroxyl and carbonate. In PROX treatment the peaks of mixed oxide shifted to higher BE, the concentration of hydroxyls and carbonate increased in both samples. The re-oxidation after PROX restored the original state also in this spectral region. The samples contained graphitic or hydrocarbon type carbon and carbonates. The amounts of the latter increased, and the former decreased in PROX conditions. The C 1s spectra in mixed oxide were somewhat more intense, but anyway they were similar in CoOx\_2 and 5Mn5CoOx.

### 3.2 Catalytic study of the Co-, Mn and mixed MnCo-oxide samples

In the following we report the results of catalytic study of the samples described above. Temperature programmed catalytic tests running several heating-cooling cycles were performed in NO+CO reaction (30 mg catalyst, 15 ml/min 0.66%NO+0.66%CO/He, 10°C/min.) and in PROX reaction (typically 20 mg catalyst, 20 ml/min 1%CO+1%O<sub>2</sub>+60% or 50% H<sub>2</sub>/He, 6°C/min. typically up to 250°C, 250°C/10 min isotherm before cooling down) followed by CO oxidation between the same conditions but in absence of hydrogen. In PROX reaction also stability tests were performed in isothermal conditions. The reaction mixtures were analysed by QMS, in case of PROX it was complemented with GC analysis. In NO+CO reaction the conversion of NO was compared. The catalytic performance in PROX process was described and compared by conversion of O<sub>2</sub> ( $\chi_{O_2}$ ), CO ( $\chi_{CO}$ ), conversion of CO into CO<sub>2</sub> ( $\chi_{CO_2}$ ) and into CH<sub>4</sub> ( $\chi_{CH_4}$ ) and selectivity of O<sub>2</sub> conversion into CO<sub>2</sub> ( $S=\chi_{CO_2}/2/\chi_{O_2}$ ). Between the different catalytic tests the catalysts were characterized in the same apparatus by TPO and TPR measurements up to 360°C with 6°C/min. heating rate followed by 360°C/20 min isotherm period using 1% O<sub>2</sub>/He and 5% H<sub>2</sub>/Ar, respectively.

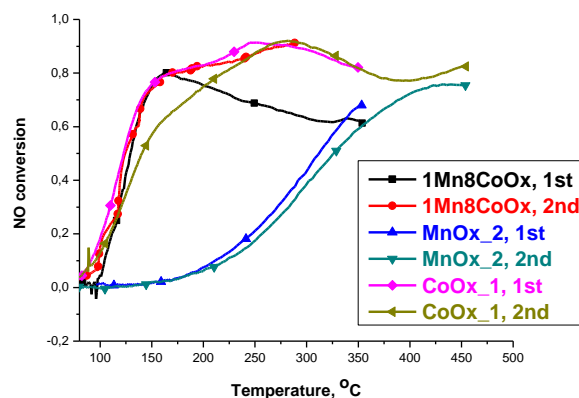


**Figure 3.15** NO conversion in NO+CO reaction on different catalyst in the cooling period of two heating cooling cycles

On Fig. 3.15 the activity of CoOx\_1, MnOx\_2 and 1Mn8CoOx can be compared in NO+CO reaction. The NO conversion in temperature programmed reaction is presented versus temperature in the cooling periods of two repeated heating-cooling runs. The Co-containing catalysts were similarly active. In the first run about 80% NO conversion was reached at already 150°C, and 90% at about 280°C. MnOx\_1 was much less active. In NO+CO reaction no synergism was observed on the mixed oxide sample, especially regarding its much higher surface area.

The catalysts were studied also in PROX reaction and CO oxidation. In Fig. 3.16 CO, O<sub>2</sub> conversion and selectivity as a function of temperature in the second heating up period of the temperature programmed PROX (TP-PROX) tests can be seen on the different catalysts. The selectivity is also shown as a function of O<sub>2</sub> conversion. In these reactions only CO<sub>2</sub> and H<sub>2</sub>O products were detected except in the case of Co-oxide, where methane formation appeared in trace amount above 240°C. The amount of catalyst used in the catalytic tests (designated in the legend of Fig. 3.16) in case of the mixed oxides and the CoOx\_2 of 31 mg provided the same catalyst surface area, that way the specific activities can be compared. The overall oxidation activity of the catalysts can be characterised by the O<sub>2</sub> conversion curves. The two Mn-oxide samples were the least active, and on the contrary that the specific surface area of MnOx\_3 composed of Mn<sub>3</sub>O<sub>4</sub> and large

amorphous part was three times higher it had similar activity as MnOx\_2 containing Mn<sub>2</sub>O<sub>3</sub> (note that the weight of this two catalysts in the PROX tests were the same). Between the mixed oxide and cobalt oxide samples no great differences can be observed. CoOx\_1 was somewhat less active, than CoOx\_2 (compare conversion curves belonging to the 20mg catalyst weight), although the specific surface area of CoOx\_2 was somewhat lower, while surprisingly the crystallite size was smaller. As expected, on 1.5 times higher amount CoOx\_2 the O<sub>2</sub> conversion reaction rate increased

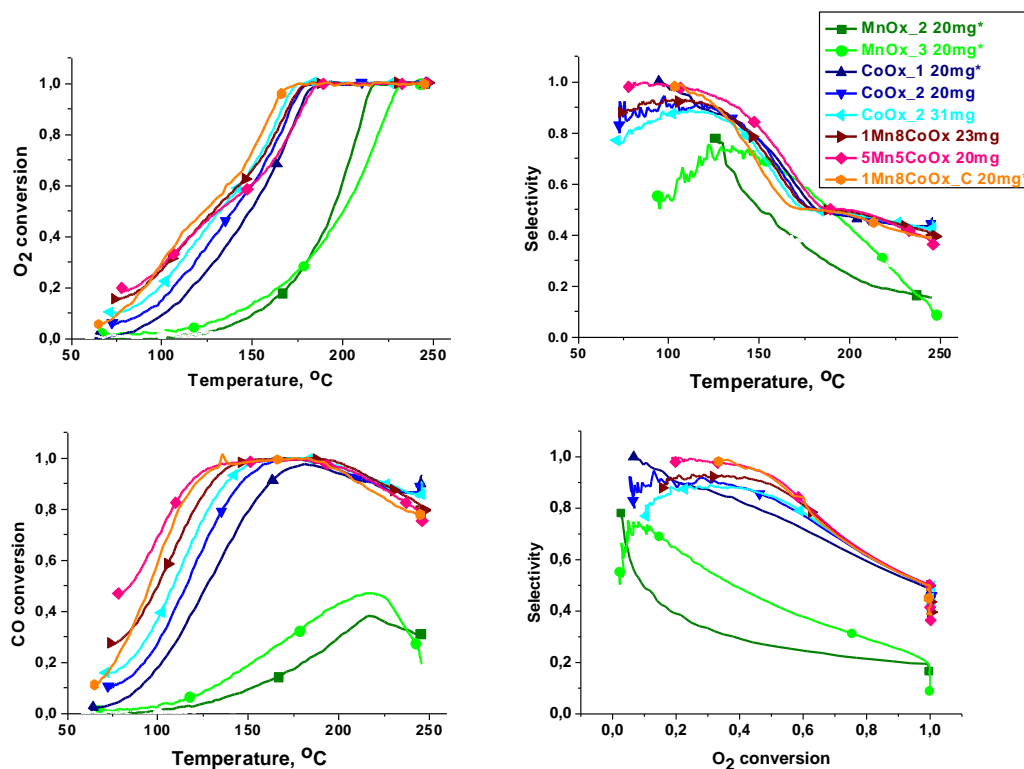


**Figure 3.16** PROX reaction in the 2<sup>nd</sup> heating up period of different samples

The catalyst amounts applied are designated.

\*The 1% CO+1% O<sub>2</sub>+H<sub>2</sub>/He reaction mixture contained 60% H<sub>2</sub> instead of 50% that was used in the other measurements

1.5 times at low conversions (below 15%). Below 125°C all three mixed oxide samples were slightly more active than CoOx\_2. The selectivity decreased with the increasing O<sub>2</sub> conversion above around 20% and with increasing temperature, in case of Co-containing samples in lower extent as 100% O<sub>2</sub> conversion had been reached. The selectivity was significantly improved in the Mn-promoted samples compared to that of pure Co-oxide. It was much lower on the MnOx samples, however, that of the Mn<sub>3</sub>O<sub>4</sub> and large amorphous part containing MnOx\_3 was somewhat larger than that of Mn<sub>2</sub>O<sub>3</sub> (MnOx\_2). Examining directly the CO conversion, it changed according to a maximum curve versus the temperature. CO conversion was clearly larger on the Mn-promoted Co-oxides than on the Co-oxides, and much more larger than on Mn-oxides. 100% CO conversion was reached on Co-containing oxides except CoOx\_1, and retained in about 30 and 15°C wide temperature region in case of mixed oxide and CoOx\_2 samples, respectively. Between the Mn-promoted Co-oxide samples some significant difference could be observed only in the lower temperature region, where CO conversion order was 5Mn5CoOx>1Mn8CoOx\_C>1Mn8CoOx, that agrees with the order of Mn/Co atomic ratio.

Fig. 3.17 shows how change the PROX performance in repeated temperature programmed reaction cycles on 5Mn5CoOx and CoOx\_2. On both catalysts both the O<sub>2</sub> and CO conversion decreased, the selectivity slightly increased in four repeated runs, and on CoOx CH<sub>4</sub> formation appeared in already in the 2<sup>nd</sup> TP-PROX cycle with increasing activity in the repeated runs. No methane formation was experienced on 5Mn5CoOx (and not on the other mixed oxide samples) even in the 12th TP-PROX cycle. The mixed oxide did not change in further six TP runs. By

temperature programmed oxidation treatment up to 360°C the original PROX performance could be restored on both catalyst as can be seen on Fig. 3.17. It should be mentioned that in PROX reaction between isothermal conditions at 165 or 150°C (not shown) no deactivation was observed during 5-6 hours on any of the mixed oxide samples and only minor deactivation on CoOx\_2.

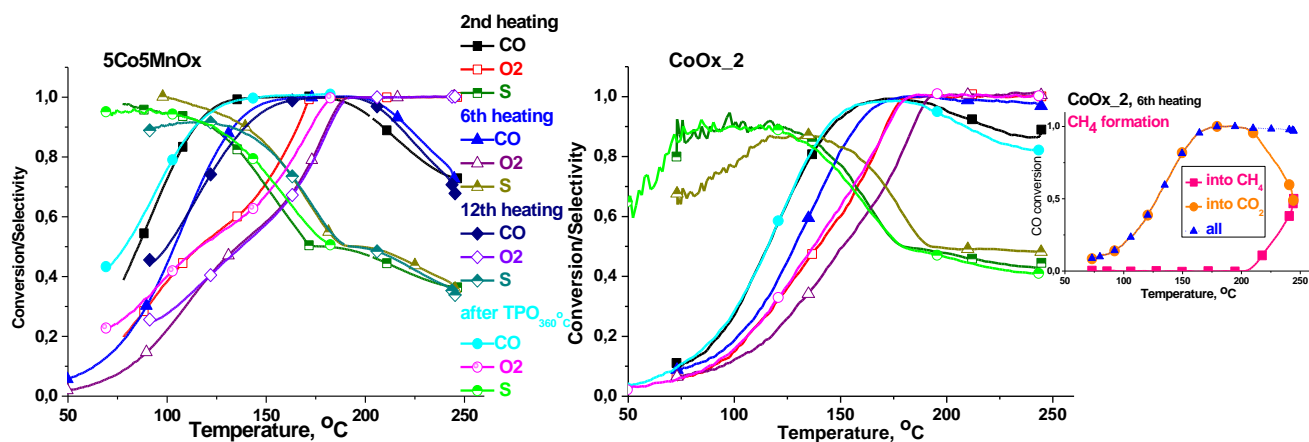


**Figure 3.17** TP-PROX in repeated heating-cooling cycles and after TPO on 5Co5MnOx (20mg) and CoOx\_2 (20mg)

The above results confirmed that the mixed MnCo-oxide catalysts possessed improved activity and selectivity in PROX reaction compared to the analogous monometallic oxide, which cannot be attributed solely the increased surface area of mixed oxide. The synergetic effect originated possibly from the partial substitution of Co by Mn ions in the  $\text{Co}_3\text{O}_4$  spinel modifying likely favourably the oxygen bond strength of key importance in the oxidation activity in reactions of Mars-van Krevelen mechanism and the competition of the CO and  $\text{H}_2$  oxidation. However, the role of the relatively high X-ray amorphous phase content of 5Mn5CoOx cannot be ruled out. Moreover, we have very limited structural information about this amorphous part. To clarify the relation between the catalytic and structural properties further experiments were performed.

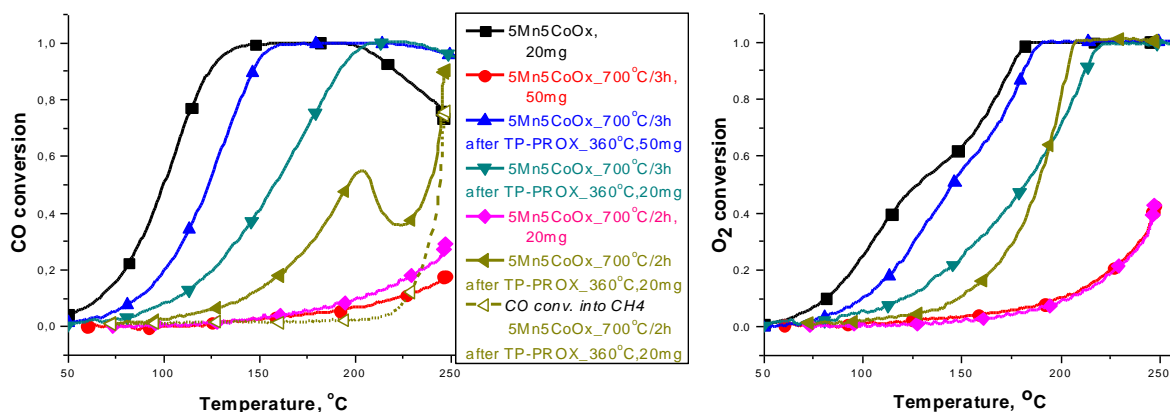


**Figure 3.18** Effect of high temperature treatment on the PROX performance of 5Mn5CoOx

The effect of high temperature treatment (700°C/2 or 3h/air) on the PROX properties of 5Mn5CoOx is demonstrated on Fig. 3.18. Astonishingly, the well crystallized 5Mn5CoOx\_700°C/3h with increased Mn substitution in the  $\text{Mn}_x\text{Co}_{3-x}\text{O}_4$  hardly showed any activity, and its selectivity was much-much lower, than that of the original sample. These changes cannot be explained by the reduced specific surface area. The 700°C treatment was repeated with

another portion of 5Mn5CoOx (5Mn5CoOx\_700°C/2h) for shorter time and the dramatic deactivation was reproduced in somewhat smaller extent. These results queried the assumption, that the improved PROX properties can be attributed to crystalline  $Mn_xCo_{3-x}O_4$ . Maybe the loss of amorphous phase and the possible decrease of irregularity, as e.g. oxygen vacancy concentration resulted in deactivation.

To probe the 5Mn5CoOx\_700°C samples the TP-PROX reaction was conducted up to 360°C, by that activity increased not only according to the kinetic temperature effect, but likely structural changes activating the catalyst were induced. Above 250°C methane formation started also on this mixed oxide. In a following TP-PROX run much higher activity was observed, similar to that of CoOx\_2 (compare the measurements of catalyst amounts providing the same surface area, CoOx\_2 of 20mg on Fig.3.17 and 5Mn5CoOx\_700°C/3h activated of 50mg on Fig.3.18). The analogous 5Mn5CoOx\_700°C/2h could be also reactivated by PROX up to 360°C, but on this reactivated sample the methane formation appeared already below 250°C and the PROX selectivity was much lower.

As was described above CoOx deactivated in repeated TP-PROX runs, while methanation activity appeared. Methane formation activity developed also on the mixed oxide samples if PROX was conducted up to 360°C. The activity could be restored by temperature programmed oxidation treatment up to 360°C (remember that TPO up to this temperature was applied in preparation of the samples). Fig. 3.19 presents the O<sub>2</sub> conversion during these TPO treatments of the different catalysts.

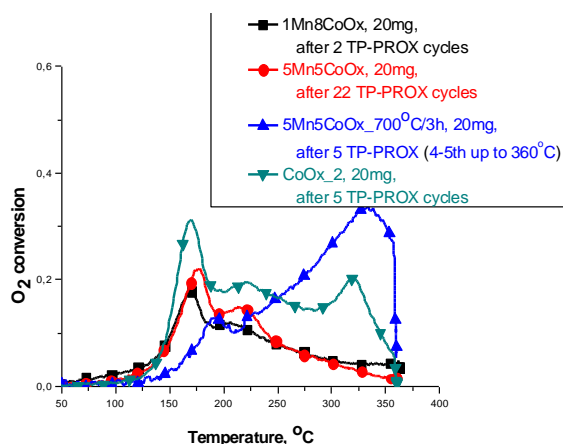


**Figure 3.19** TPO on different Co-containing catalysts after PROX reactions  
conditions: 20ml/min 1%O<sub>2</sub>/He, 6°C/min

CoOx\_2 and the mixed oxide 1Mn8CoOx and 5Mn5CoOx consumed O<sub>2</sub> indicating that these samples had been reduced during PROX treatments in different extent, CoOx\_2 in the highest, the mixed oxides in smaller extent, except of 5Mn5CoOx\_700°C/3h that reduced more in PROX up to 360°C. The profile of the TPO curves of the original samples after several TP-PROX measurement was similar showing a peak with maximum at 170-175°C, and smaller, wider one at 205-220°C, but in case of CoOx\_2 there was an extra, wide band with maximum at 335°C. Also 5Mn5CoOx\_700°C used in higher temperature PROX presented this latter TPO band of higher intensity than CoOx\_2, while the two lower temperature peaks were smaller and shifted slightly to higher temperatures, than in case of the other mixed oxide samples. The high temperature TPO peak was characteristic of the samples producing methane in PROX reaction conditions.

The effect of 700°C/2h/air treatment and the extent of reduction of the catalyst in TP-PROX reaction and other treatments was studied also on the 1Mn8CoOx sample (see Fig. 3.20 and Fig. 3.21, respectively).

The treatment at 700°C in air decreased the activity of 1Mn8CoOx in much less extent, than that of 5Mn5CoOx, while the selectivity did not change significantly, not as for 5Mn5CoOx. The

surface area of 1Mn8CoOx\_700°C/2h was 30m<sup>2</sup>/g, only 1.5 times higher than that of 5Mn5CoOx\_700°C/3h. The TP-PROX up to 360°C, what activated the 5Mn5CoOx\_700°C/2 and 3h, deactivated further this catalyst, decreased slightly the PROX selectivity and developed methanation activity also in this case. A TPO treatment after all these reactivated indeed the samples, the activity in the low conversion range was about 20-25% of the original sample that is smaller than could be expected regarding only the reduction of surface area (40-45%).

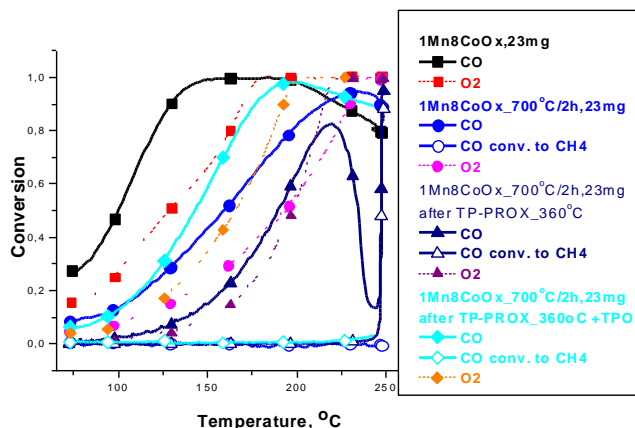


**Figure 3.20** Effect of high temperature treatment on the PROX performance of 1Mn8CoOx

The TPO of variously treated 1Mn8CoOx reflects on the oxidation state and structure of the sample. The profile and the O<sub>2</sub> uptake are somewhat different in the different cases. Two TP-PROX cycles up to 250°C practically did not reduce the high temperature treated sample, while reduced in the smallest extent of the original sample compared to other treatments. The highest extent reductions occurred on the original sample during TPR treatment by 1% CO/He up to 360°C with 360°C/20 min isotherm period, and on 1Mn8CoOx\_700°C/2h in TP-PROX up to 360°C. These samples had methanation activity and could be re-oxidised at around 330°C. Remarkably the TPR by 1%H<sub>2</sub>/Ar up to 360°C followed by 360°C/20min isotherm period did not reduce the original sample in such a high extent, and TP-PROX up to 250°C following a H<sub>2</sub>-TPR treatment could further reduce the catalyst.

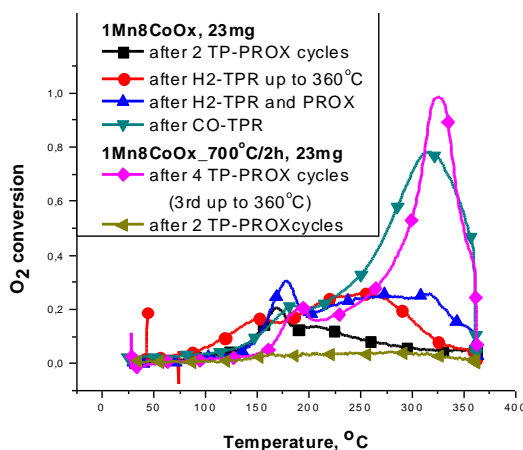


**Figure 3.21** TPO of 1Mn8CoOx and 1Mn8CoOx\_700°C/2h after PROX reactions and other consecutive treatments conditions: 20ml/min 1%O<sub>2</sub>/He, 6°C/min

Fig. 3.22 demonstrates the effect of 700°C/air treatment on the catalytic performance of CoOx<sub>2</sub>. The behaviour of this catalyst, CoOx<sub>2</sub>/700°C/2h is more similar to that of

1Mn8CoOx\_700°C/2, than to 5Mn5CoOx\_700°C/2 or 3h. Namely, there was no such tremendous deactivation of the original catalyst observed as in case of the latter samples. The total oxidation and CO oxidation activity (reaction rate of O<sub>2</sub> and CO consumption, respectively, estimated at low conversions) of CoOx\_700°C/2h was about 15-20% of activity of the original CoOx\_2, while its specific surface area was 20% of that of CoOx\_2. So the activity decrease can be attributed dominantly to the surface area reduction. Presumably besides sintering no other structural changes occurred during high temperature treatment. Similarly to 1Mn8CoOx\_700°C/2h a TP-PROX treatment up to 360°C did not increase, but oppositely decreased the activity of CoOx\_2/700°C/2h accompanied by increasing methanation activity. By a TPO treatment up to 360°C the activity of CoOx\_2/700°C/2h could not only be restored, but slightly increased. The activity estimated at low conversions was around 25-30% of that of CoOx\_2. The specific surface area of this sample was not measured.

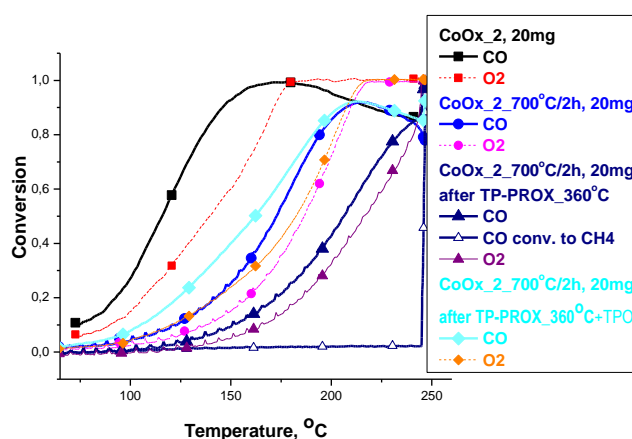


**Figure 3.22** CO and O<sub>2</sub> conversion in PROX after different treatments on CoOx<sub>2</sub>

TPO of variously treated CoOx<sub>2</sub> samples are presented on Fig. 3.23. The mechanical mixture of CoOx<sub>2</sub>+MnOx<sub>3</sub> after 3 TP-PROX cycles have similar TPO profile as CoOx<sub>2</sub> after 5 TP-PROX with lower intensity (CoOx<sub>2</sub> weight in the catalytic tests was the same), likely because of the less use in PROX reaction. Remember that CoOx<sub>2</sub> were reduced in higher extent than the mixed oxides in PROX reaction. The CoOx<sub>2</sub> treated at 700°C was reduced severely in the high temperature TP-PROX up to 360°C, which could be re-oxidized dominantly on higher temperature (see that TPO peak centred at 170°C decreased, the other above 300°C strongly increased).

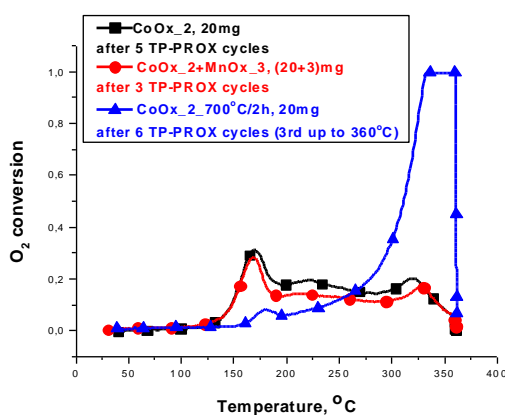


**Figure 3.23** TPO of CoOx<sub>2</sub> and mechanical mixture of CoOx<sub>2</sub> and MnOx<sub>3</sub> (20+3mg) after different treatments conditions: 20ml/min 1% O<sub>2</sub>/He, 6°C/min

The reducibility of CoOx\_2 and 1Mn8CoOx can be compared also by the TPR curves collected on Fig. 3.24. CoOx could be reduced at lower temperature and higher extent, than the mixed oxide sample. It is noteworthy that on the effect of treatment at 700°C the reducibility of the mixed oxide increased, however did not reach that of CoOx\_2.

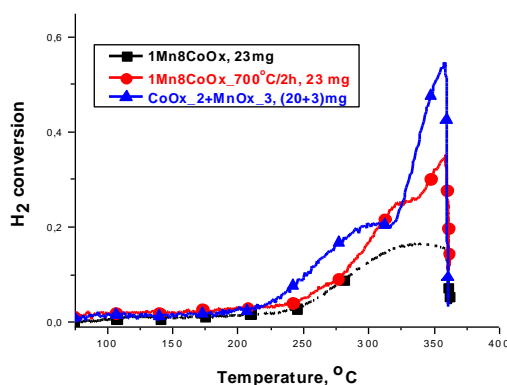


**Figure 3.24** TPR of 1Mn8CoOx and mechanical mixture of CoOx\_2 and MnOx\_3 after TPO (+360°C/20min/1% O<sub>2</sub>/He) treatments.  
conditions: 20ml/min 5% O<sub>2</sub>/H<sub>2</sub>, 6°C/min

The TPO measurements revealed that in the TP-PROX tests up to 250°C the pure Co-oxide samples were reduced irreversibly much more, than the MnCo-oxide samples. In the Co-oxide this reduction formed sites having methanation activity. According to XPS investigations these sites were not metallic Co, but presumably ordered, crystalline CoO that can be re-oxidized only at relatively high temperature, above 300°C. Such sites formed in the mixed oxide catalysts only above 250°C in PROX mixture or 5% H<sub>2</sub>/Ar. Both the smaller and the deeper irreversible reduction in the course of the PROX reaction decreased the activity of the catalyst, what could be restored by re-oxidation of the catalysts.

The main results of the research work on mixed MnCo- and pure Co- and Mn-oxide and their application in the preferential oxidation of CO in presence of hydrogen can be summarized as follows.

- In CO oxidation and PROX reaction the activity and selectivity of the 3 mixed MnCo-oxides (Mn/Co: 5/95, 8/92, 12/88, respectively) containing Mn-substituted Co<sub>3</sub>O<sub>4</sub> besides some amount of X-ray amorphous phase were similar to each other and were higher than that of CoOx composed of Co<sub>3</sub>O<sub>4</sub> (comparing catalytic tests of catalyst amount with the same surface area). MnOx was the least active and selective. CO oxidation activity was lower in presence of H<sub>2</sub> suggesting competitive catalytic oxidation of CO and H<sub>2</sub>.
- The higher activity of mixed oxides seemed to be originated from the Mn-substitution in Co<sub>3</sub>O<sub>4</sub> likely modifying favourably the binding energy of lattice oxygen. However after high temperature treatment, in more crystallized and somewhat sintered form of the Mn<sub>z</sub>Co<sub>3-z</sub>O<sub>4</sub> were less active than Co<sub>3</sub>O<sub>4</sub> (also if the activities were related on the same surface area). In the same high temperature treatment CoOx were sintered in higher extent than mixed oxides, but its activity decreased according to the surface area reduction.
- In several repeated TP-PROX runs mixed oxides and CoOx deactivated somewhat, while the temperature range of 100% CO conversion narrowed for mixed oxides, but widened for CoOx. The latter was not caused by increase of CO conversion into CO<sub>2</sub> but by evolving methanation activity likely due to partial reduction of cobalt.
- TPO, XAS and XPS confirmed that the mixed oxides and CoOx were partially reduced in the course of PROX reaction that decreased their activity. XPS studies showed significant increase of hydroxyl, water and carbonate surface concentration on the mixed oxides, and CoOx, and in

less extent on MnO<sub>x</sub> even at low reactant pressure at 140°C. By re-oxidation the activity could be restored.

#### 4. Study of SiO<sub>2</sub>/Si(100) supported Ag and Au and AgAu thinfilm and nanoparticle systems

These investigations have been started in the former NNF-77837 project. Fe covered Au/Ag inverse model system (Fe/Au<sub>y</sub>Ag<sub>z</sub>/SiO<sub>2</sub>/Si(100)) were prepared by molecular beam epitaxy (MBE) using co-evaporation of Ag and Au followed by Fe evaporation. The thickness of the Fe deposit was 0, 10 or 40 nm, and that of Au<sub>y</sub>Ag<sub>z</sub> (z:y= 100:0, 80:20, 50:50, 20:80 and 0:100) was 30 nm, in case of pure Ag layer also 5 and 20 nm. After evaporation the samples were kept in air for oxidation of Fe layer. All of the samples were tested in CO oxidation reaction. The catalytic activity depended on the Au-Ag ratio; the silver-rich catalysts were significantly more active than the gold-rich ones with or without FeO<sub>x</sub> overlayer. The increasing catalytic activity was nearly linear with the Ag/Au ratio, which means there was no synergism between the gold and silver in CO oxidation reaction.

In the recent project additional synchrotron radiation excited photoelectron spectroscopy, conventional photoelectron spectroscopy (XPS, UPS) and X-ray diffraction studies were used for more detailed characterization of the model samples prepared and already investigated in the former project.

As can be seen in the Fig. 4.1 a and b, the size dependence of Ag 4d valence band density of states is mostly noticeable at lower binding energies (3-6 eV) according to the formation of Cooper minimum of the energy distribution curve's (EDC) data obtained in 30-150 eV exciting photon energy range.

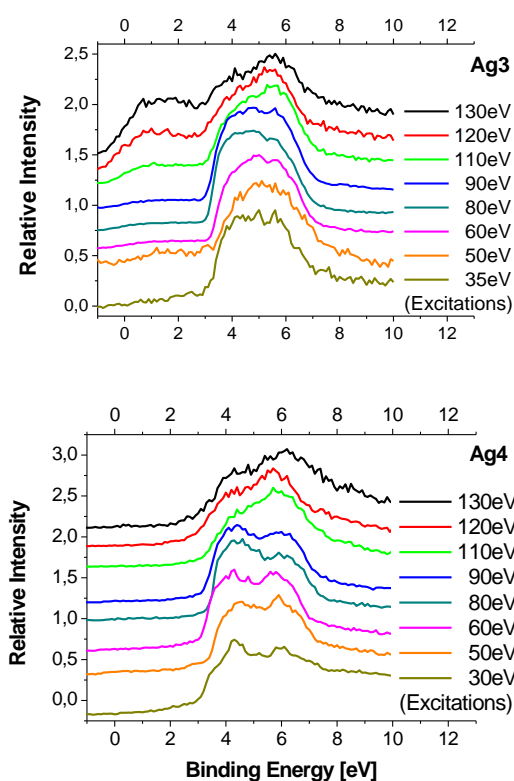


**Figure 4.1** Synchrotron radiation excited photoelectron spectra of 5 nm Ag/SiO<sub>2</sub>/Si(100) (upper diagram „Ag3”) and 20 nm Ag/SiO<sub>2</sub>/Si(100) (lower diagram „Ag4”)

On UPS spectra (HeI excitation, 20eV) we also observed significant difference in valence band of 5nm Ag/SiO<sub>2</sub>/Si(100) as compared to the 20nm Ag/SiO<sub>2</sub>/Si(100) having typical bulk Ag valence band as can be seen on Fig. 4.2.

In Au<sub>20</sub>Ag<sub>80</sub> the Ag 4d originated valence band density of states (DOS) seems to be modified (Fig. 4.3). This is mostly in the same B.E. energy region as in case of nanosize effect, however the modification is smaller. The Au<sub>80</sub>Ag<sub>20</sub> alloyed layer shows rather the superposition of the valence band spectra of Au and Ag, namely Ag 4d originated DOS is not modified by alloying with Au.

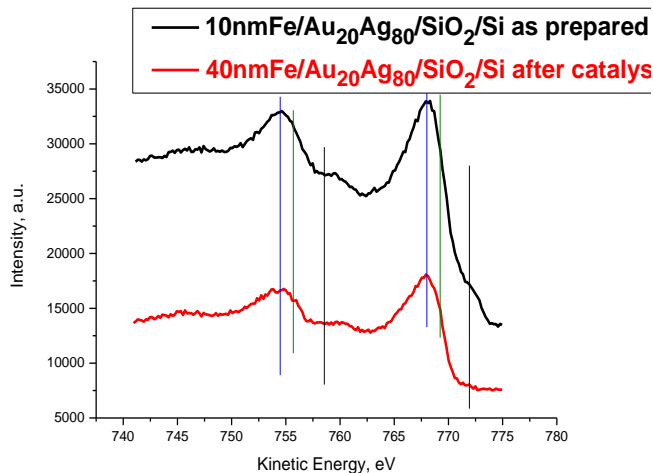


**Figure 4.2** UPS spectra of (a) 5 nm Ag/SiO<sub>2</sub>/Si(100) and (b) 20 nm Ag/SiO<sub>2</sub>/Si(100)

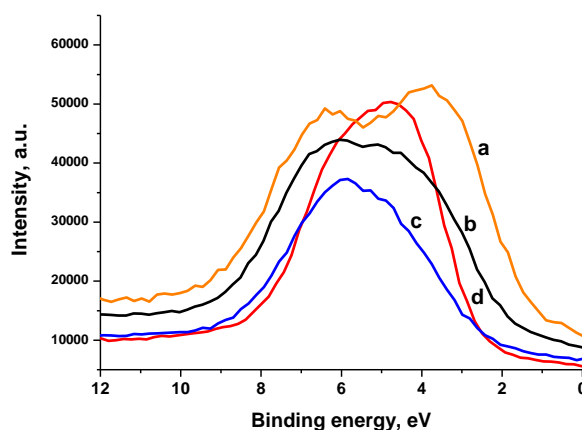


**Figure 4.3** Valence band spectra of Au and Ag on the (a) Au/SiO<sub>2</sub>/Si(100), (b) Au<sub>80</sub>Ag<sub>20</sub>/SiO<sub>2</sub>/Si(100), (c) Au<sub>20</sub>Ag<sub>80</sub>/SiO<sub>2</sub>/Si(100) and (d) Ag/SiO<sub>2</sub>/Si(100) samples (thicknesses of the created layers were 30 nm)

We characterised the FeO<sub>x</sub> covered samples also by XPS and XRD. On Fig. 4.4 Ag can be observed with low intensity on the 10nm FeO<sub>x</sub> covered samples in as prepared state and after catalytic test even on the 40nm FeO<sub>x</sub> covered samples. Ag/Fe atomic ratio is less than 15/85. Ag concentration on the top surface must be even lower compared to Fe, it is rather in the subsurface layers. Indeed, in "top" surface sensitive mode (see inset of Fig. 4.4) Ag cannot be detected on the 40nm FeO<sub>x</sub> covered samples even after catalytic test. It means that Ag (and Au) are not exposed to the surface. Fe overlayer due to atmospheric oxidation is transformed into FeO<sub>x</sub> in as prepared state, which is composed of Fe<sub>2</sub>O<sub>3</sub> (Fe<sup>3+</sup>), FeO (Fe<sup>2+</sup>), FeOOH and some metallic Fe. After catalytic test similar composition except no metallic Fe is detected.

As can be seen on Fig. 4.6 XRD also confirmed the presence of metallic Fe in the as prepared state, FeO<sub>x</sub> (clearly observed by XPS) was not detected, it must be X-ray amorphous.

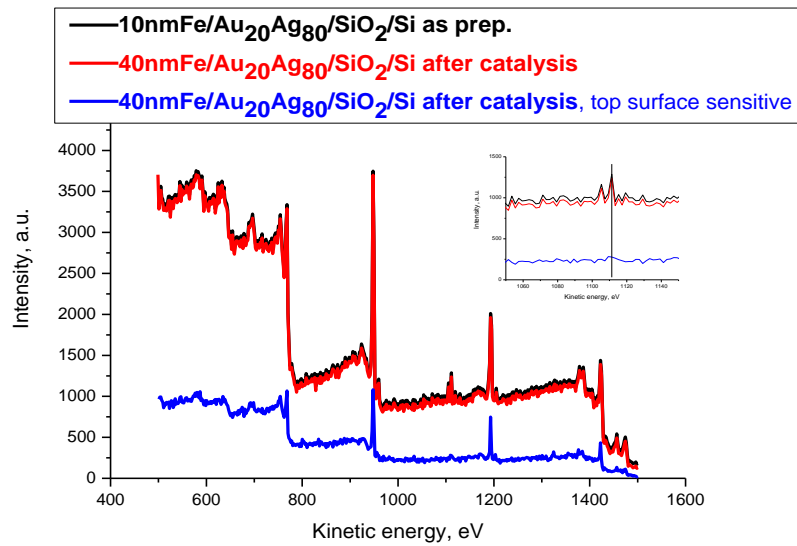


**Figure 4.4** XPS spectra of different Fe/AuAg/SiO<sub>2</sub>/Si(100) samples ( $E_f=1478.6$  eV), Ag 3d region is magnified in the inset.

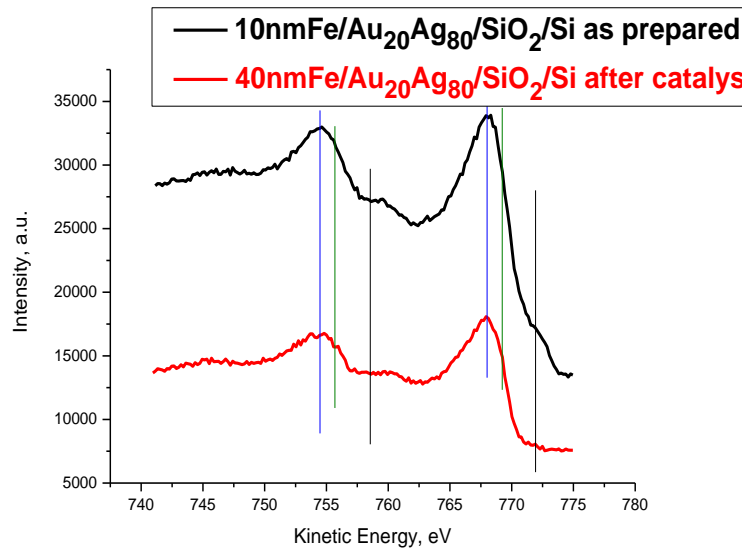


**Figure 4.5** Fe 2p<sub>3/2</sub> XPS spectra of Fe/20Ag80Au/SiO<sub>2</sub> ( $E_f=1478.6$  eV) (Blue, green and black lines indicate the position of peaks belonging to Fe<sup>3+</sup>, Fe<sup>2+</sup> and Fe<sup>0</sup>)

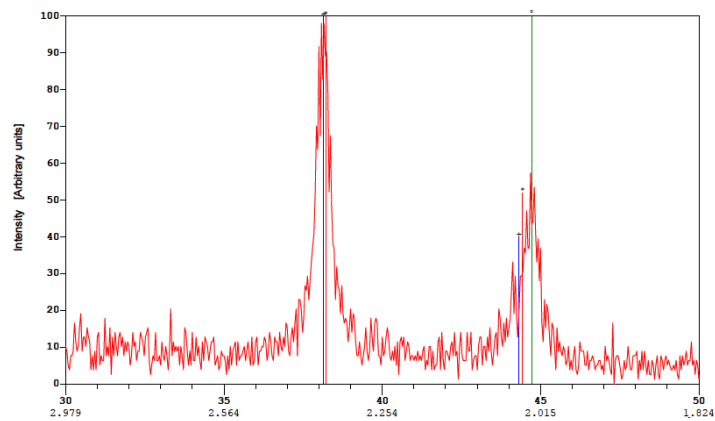


**Figure 4.6** XRD of 40Fe/20Au80Ag/SiO<sub>2</sub>/Si

Based on the additional results gained in this project we can conclude that the changes in the Ag 4d valence band density of states observed in 5nm Ag/SiO<sub>2</sub>/Si(100) in comparison with typical bulk Ag VB of 20nm Ag/SiO<sub>2</sub>/Si(100), accompanied with increased catalytic activity in CO oxidation reaction. Alloying Ag with Au resulted also in some smaller changes of these Ag 4d valence band states (3-6 eV) at the Ag rich Au<sub>20</sub>Ag<sub>80</sub> composition, but no significant changes were discerned in the Au rich Au<sub>80</sub>Ag<sub>20</sub>. On the contrary in the CO oxidation catalytic activity of the AuAg/SiO<sub>2</sub>/Si(100) samples were between those of the monometallic samples and decreased with the increasing Au/Ag ratio of the alloy, and Au<sub>20</sub>Ag<sub>80</sub>/SiO<sub>2</sub>/Si(100) having modified valence band did not show dissimilar activity. No obvious synergetic effect on the activity was observed.

The catalytic activity of the continuous FeO<sub>x</sub> overlayer on Ag(Au)/SiO<sub>2</sub>/Si(100) samples were higher than that of FeO<sub>x</sub> over SiO<sub>2</sub>/Si(100). This shows the clear promotion of Ag or AuAg on the activity of FeO<sub>x</sub> overlayer. This promotion effect depended on the thickness of FeO<sub>x</sub> overlayer, the nano or bulk character of Ag and composition of AuAg alloy.

## 5. High surface area SiO<sub>2</sub> supported bimetallic AgAu system

High surface area silica supported AuAg bimetallic catalysts and the monometallic analogous ones were prepared by adsorption of metal colloids and tested in CO oxidation and selective glucose oxidation reactions in the preceding OTKA #NNF-77837. The CO oxidation activity of the bimetallic systems was low, however synergetic effect was observed in the latter reaction. In the frame of the present project more detailed structural and catalytic investigations in the glucose oxidation were performed on these catalytic systems.

### 5.1 Structure of the AgAu/SiO<sub>2</sub> catalysts

Table 1 presents AgAu particle sizes of the catalysts samples after calcination at 400°C in synthetic air (by that the organic residues can be removed) and after following reductive treatment in H<sub>2</sub> at 350°C determined by TEM and the standard deviations which are characteristic of the particle size distribution. The mean particle size of pure Au/SiO<sub>2</sub> and pure Ag/SiO<sub>2</sub> sample were similar, 4.8nm. In the case of Ag/SiO<sub>2</sub> sample the particle size distribution was broad (4.8 ± 3.5 nm) due to several much larger particles with 5-16nm in diameter beside the numerous particles with 3-4nm size. In the case of the bimetallic samples the particle sizes range between 2.9 and 5.2nm and the samples were stable against sintering. Small changes were observed in the particle sizes after reduction treatments (or catalytic reaction), and the resulting sizes were more similar in the different samples than in the calcined state.

**Table 5.1** Particle sizes of the catalysts samples determined by TEM

Catalysts	Particle size determined by TEM (nm)		
	after calcination	after reduction	after reaction
Au/SiO <sub>2</sub>	4.8 ± 2.4	4.0 ± 2.0	-
10Ag90Au/SiO <sub>2</sub>	3.5 ± 2.3	3.1 ± 1.6	3.5 ± 2.0
20Ag80Au/SiO <sub>2</sub>	2.9 ± 1.2	3.5 ± 1.7	-
33Ag67Au/SiO <sub>2</sub>	3.4 ± 2.5	3.3 ± 1.2	-
50Ag50Au/SiO <sub>2</sub>	5.2 ± 2.2	-	-
Ag/SiO <sub>2</sub>	4.8 ± 3.5	4.9 ± 3.6	-

HRTEM of monometallic calcined Ag/SiO<sub>2</sub> sample is shown in Figure 5.1. Fringe periods of both Ag (2.03Å, 2.35Å, 2.37Å) and Ag<sub>2</sub>O/Ag<sub>2</sub>O<sub>3</sub> (2.49Å) can be identified in the catalyst after calcination in air at 400°C. Only a few crystals were found as Ag<sub>2</sub>O/Ag<sub>2</sub>O<sub>3</sub>, most part of the particles was in metallic state. It is worth pointing out that both Ag and Ag<sub>2</sub>O/Ag<sub>2</sub>O<sub>3</sub> phases were presented within a particle (Figure 5.1) regardless of whether they were small or large particles. HRTEM measurement of calcined 33Ag67Au/SiO<sub>2</sub> catalyst showed mostly metallic crystals and phase contrast was not observed within the particles.

Figure 5.2 shows the UV-Vis spectra of the supported catalysts after calcination (a) and after reduction treatment (b). The intensities of the bands are not comparable because - as a consequence of the measurement method - the catalyst amounts placed on the glass plates were not the same. Single adsorption bands were detected in the case of all samples after calcination, except of 20Ag80Au/SiO<sub>2</sub> catalysts where the spectrum reveals two bands, both of them positioned between the pure Ag and Au bands suggested some phase-segregated structure. All surface plasmon resonance (SPR) bands were broad due to - considering the TEM results - the small diameters of the particles. After reduction only single, narrower SPR bands were detected for all catalysts compared to the bands of the calcined samples.

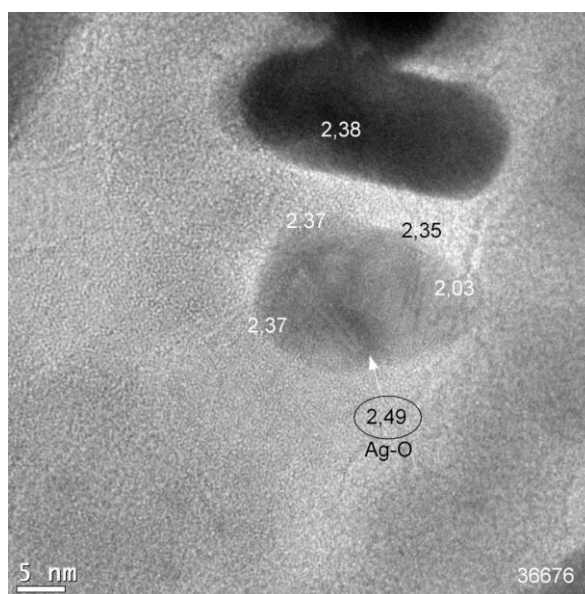


**Figure 5.1** HRTEM of Ag/SiO<sub>2</sub> calcined at 400°C

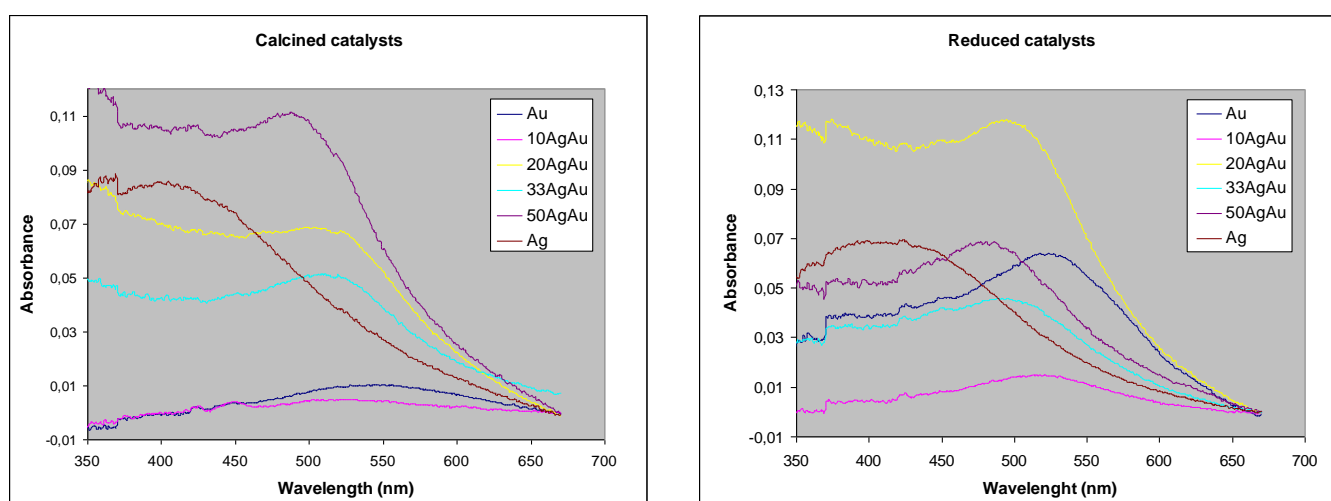


**Figure 5.2** UV-Visible spectra of AgAu/SiO<sub>2</sub> catalysts (a) after calcination in air at 400°C  
(b) after reduction in H<sub>2</sub> at 350°C

Figure 5.3 a and b show the correlation between the nominal Au molar ratio and the maximum of surface plasmon bands. The SPR bands shift to higher wavelengths with increasing Au molar ratio. The position of the maximum absorption band is related to the surface structure and composition beside the particle size. Linear correlation was found in the case of calcined samples and reduced samples suggesting Ag-Au alloy structure in accordance with the literature. The band positions were changed with calcination-reduction treatments. In the calcined samples deviation from linearity can be originated from the somewhat different particle size and may suggest some phase segregation, not a homogeneous alloy. Reduction pretreatment caused a blue shift of the absorption bands and a diminution of the deviation from linearity suggesting homogeneous Au-Ag alloy structures. This effect could be explained by the following: oxygen treatment favors the Ag enhancement on the surface because Ag-oxide formation is thermodynamically favored, but as the temperature rises the decomposition of the preformed oxide is occurred above 280°C. Modification of the surface plasmon of the particles likely reflects this surface structure/geometry change, that can be an important factor affecting the catalytic properties.

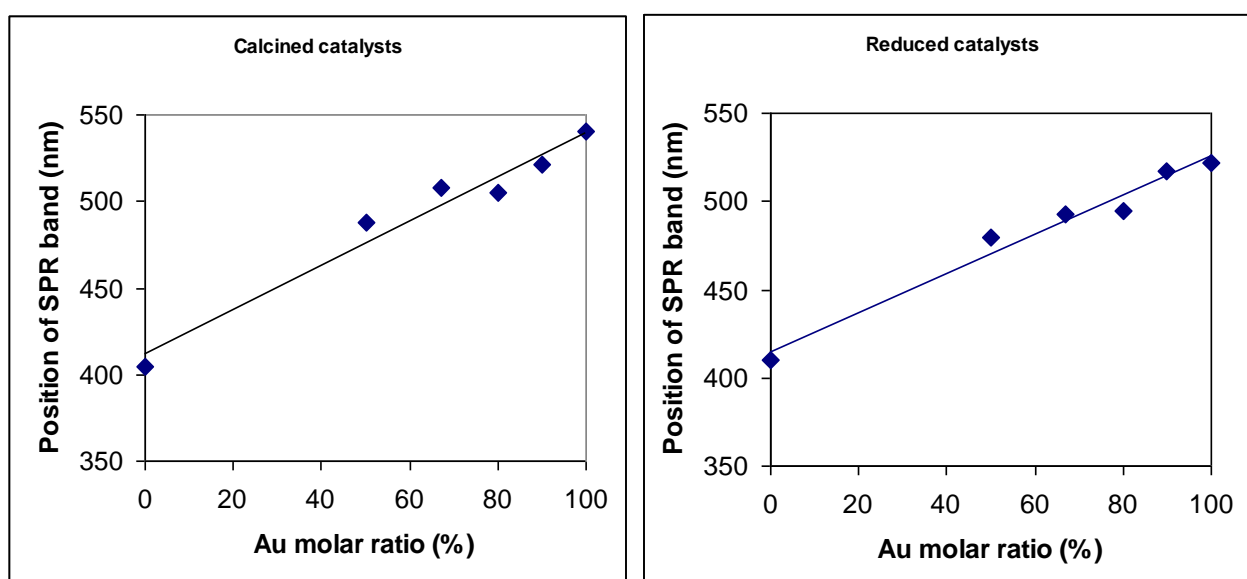


**Figure 5.3** UV-Vis absorption band maximum of AgAu/SiO<sub>2</sub> catalysts versus Au molar fraction after calcination in air at 400°C (a) and after reduction in H<sub>2</sub> at 350°C (b)

**Table 5.2** XPS data of AgAu/SiO<sub>2</sub> catalysts

Catalysts	Au binding energy (eV)		Ag binding energy (eV)		Ag/Au at. ratio		
	calcined catalysts	reduced catalysts	calcined catalysts	reduced catalysts	nominal	calcined catalysts	reduced catalysts
Au/SiO <sub>2</sub>	83	83	-	-	-	-	-
10Ag90Au/SiO <sub>2</sub>	82.9	82.8	367	366.8	0.11	0.18	0.17
20Ag80Au/SiO <sub>2</sub>	82.9	82.8	367.5	367.3	0.25	0.34	0.28
33Ag67Au/SiO <sub>2</sub>	82.9	83.2	367	367.1	0.5	1.14	1
50Ag50Au/SiO <sub>2</sub>	82.9	83.1	367.4	367.3	1	1.17	1.17
Ag/SiO <sub>2</sub>	-	-	368.6	367.2	-	-	-

XPS spectra were recorded on the catalyst samples after calcination in air at 400°C and after reduction treatment in H<sub>2</sub> at 350°C. Table 5.2 shows the binding energies of Au 4f<sub>7/2</sub> and Ag 3d<sub>5/2</sub>. BE of Au was in the range of 82.9 – 83.2eV which can be assigned to Au metallic state. Combining Au with Ag the BE of Ag shifts to lower value (366.8 – 367.5eV) from 368.6 eV measured for

Ag/SiO<sub>2</sub> sample. The effect of reduction treatment on the BE was smaller and not really significant in the case of bimetallic catalysts than in the case of pure Ag/SiO<sub>2</sub> in case of that the BE of Ag 3d<sub>5/2</sub> decreased by 0.6eV.

In the case of the bimetallic samples the BE of Au was lower compared to the 84.0eV typical for metallic Au according to the literature but the shifts were not significant compared to that determined on the monometallic Au/SiO<sub>2</sub> sample. In the case of the calcined samples the BE of Au did not change with the Ag content. After reduction practically no change in the BE of Au was observed in the bimetallic samples at 10% and 20% Ag-content and small shift to the higher BEs occurred in the 33% and 50% Ag-content samples. The small negative shift of Au BE in the samples suggests a tiny negative charge excess on Au. On the other hand in the bimetallic samples BE of Ag 3d<sub>5/2</sub> were shifted to lower values compared to the metallic silver (368.3eV) which – according to the well reported and accepted anomalous XP spectroscopic behavior of Ag - indicates positively charged Ag. The electron transfer from Ag to Au could cause BE shifts in the bimetallic samples. However, the clear shift of Ag 3d<sub>5/2</sub> band to lower BE in the monometallic Ag/SiO<sub>2</sub> as a result of reducing treatment is in contradiction with the general view about behavior of Ag and our other results.

The surface atomic ratio of Ag and Au were calculated and presented in Table 5.2. Surface Ag/Au ratios are slightly higher than the bulk nominal Ag/Au ratio, except of 33Ag67Au/SiO<sub>2</sub> sample, in this case high Ag enrichment on the surface was observed.

### 5.2 Catalytic properties in glucose oxidation

Bimetallic Ag-Au/SiO<sub>2</sub> catalysts with different Ag-Au ratios were tested in glucose oxidation. The catalytic activity of the samples was compared in Figure 5.4. Synergistic activity increase was achieved with addition of Ag to Au at lower than Ag/Au=1/1 atomic ratio. The activity reached a maximum value at 20% Ag content. Regarding that the mean particle size of the bimetallic particles is the smallest (2.9nm) also in the 20Ag80Au/SiO<sub>2</sub> sample, it does not mean that the 20/80 is the optimum atomic ratio but is is rather smaller. At 50% nominal Ag content no activity was detected as in the case of pure Ag/SiO<sub>2</sub> sample. The inactivity of 50Ag50Au/SiO<sub>2</sub> cannot be explained only by the largest particle size (5.2nm), the Ag/Au ratio must be a more important factor.

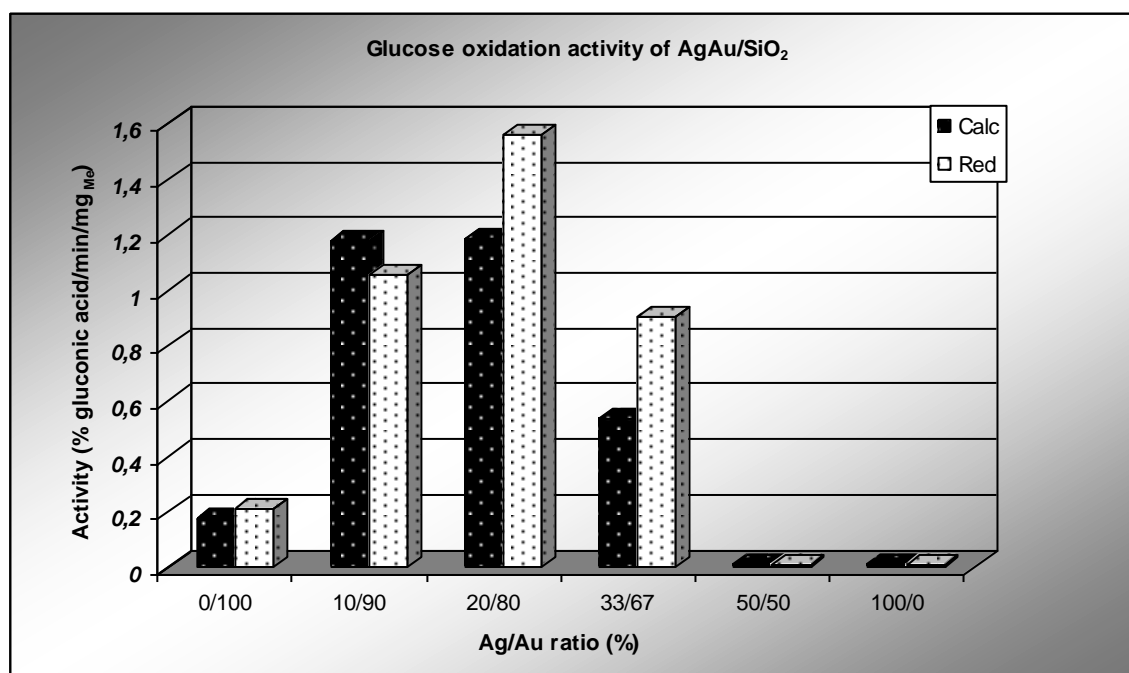


**Figure 5.4** Catalytic activities of the AgAu/SiO<sub>2</sub> samples in glucose oxidation; T=35°C, pH 9.5, c<sub>glucose</sub> =0.1M

Stability of the samples was studied by repeating the catalytic measurement after 1 year of sample storage. Experiments showed high stability, similar activities were achieved in the case of all samples. The effect of the reduction treatment in H<sub>2</sub> at 300°C of the calcined samples was investigated. The reduction treatment slightly affects the activity of the calcined 10Ag90Au/SiO<sub>2</sub> and Au/SiO<sub>2</sub> catalysts, while the particle size decreased somewhat. The 50Ag50Au/SiO<sub>2</sub> and Ag/SiO<sub>2</sub> showed no activity even in reduced form. In case of 33Ag67Au/SiO<sub>2</sub> and 20Ag80Au/SiO<sub>2</sub> the reduction increased the activity in a higher and somewhat lower extent, respectively, on the contrary that in 20Ag80Au/SiO<sub>2</sub> the particle size increased to 3.5nm during the treatment in hydrogen. These differences might be explained by the decreased surface Ag/Au atomic ratio in the latter reduced samples supposing that the optimal Ag/Au surface ratio is below that in calcined 20Ag80Au/SiO<sub>2</sub>.

Summarizing, Ag addition to Au/SiO<sub>2</sub> up to about Ag/Au= 0.5 provided synergetic effect in selective glucose oxidation reaction. The AgAu catalysts contained dominantly alloyed metallic particles both after calcination and following reduction treatments. The calcination – reduction pretreatment changing somewhat the particle size and the surface Ag/Au atomic ratio slightly affected the activity of the catalysts, however, the activity order of the samples remained the same. The higher activity of the bimetallic samples could be due to the improved O<sub>2</sub> activating ability provided by Ag sites. The further increase of Ag loading above the optimal concentration may dilute the Au to such an extent that the population of extended gold surface necessary for glucose activation decreases deteriorating the activity.

## 6. Summary

The research carried out in the frame of OTKA project #NNF2-85631 was not fully conform to the research plan. In the latter the study of Mn- and Co-oxide supported Au, Ag and bimetallic AgAu systems as possible alternative of Pt, Pd, Rh containing catalysts in CO oxidation and NO reduction by CO as model reaction for automotive exhaust gas abatement processes were proposed. The activity in this project was dominantly the continuation of the work commenced and could not be completed in the preceding #NNF-78837 2 years project. These work proceeded towards the aim foreseen in the research plan, but we could not start the investigation of the AuAg/MnO<sub>x</sub> and CoO<sub>x</sub> systems in the timeframe of the project, because the investigation of the two active components, namely bimetallic AuAg and MnO<sub>x</sub>/CoO<sub>x</sub> separately seemed to be reasonable first. The study of the oxalate derived MnO<sub>x</sub> system was widened further, see the results in chapter 1, and it was complemented with the preparation and characterization CoO<sub>x</sub> and MnCoO<sub>x</sub> mixed oxide. Since the mixed oxides presented synergetic effect in CO oxidation and CO preferential oxidation in hydrogen (PROX) but not in NO+CO reaction, their catalytic investigation was focused on the former process. Research on this field was reported in chapter 3. The behaviour of AuAg bimetallic particles on an inert support with special attention to the structural aspects were investigated more detailed both in model and high surface area systems. These results were presented in the chapter 4 and 5, respectively. The AuAg/SiO<sub>2</sub> samples were more promising in the selective glucose oxidation than in CO and NO+CO reaction, as was already experienced in the earlier project, so we paid more attention to this process.

In duration of the project unfortunately we had to face with the loss of Professor László Guzzi. We missed his great experience, work and advices very much. The implementation of the project was also affected by the child-bearing of the principal investigator as a gratifying event. On the other side the research work benefited by the cooperation with colleagues not involved in the research contract, as Prof. Norbert Kruse, Viacheslav Iablokov (Université Libre de Bruxelles), Dr. Detre Teschner (Fritz-Haber-Institut der Max-Planck-Gesellschaft), Dr. István Sajó, Olga Geszti, Dr. György Sáfrán (Research Centre of Natural Sciences, HAS), Prof. Gábor Pető, Tímea Benkó (who returned to our research group in April 2013 after maternity leave), Dr. Dávid Srankó (who joint our research group one year ago) and Dr. János Osán, (Centre for Energy Research, HAS).

The results reported in chapters 2-5 partly have been published already and several, at least 2 publications are to be submitted in the near future:

**chapter 2:** 1 oral presentation, 1 paper

Frey K., Iablokov V., Sáfrán Gy., Osán J., Sajó I., Szukiewicz R., Chenakin S. and Kruse N.: *High catalytic activity in CO oxidation over MnOx nanocrystals*, EuropaCat X, Glasgow, 2011 (oral)

Krisztina Frey, Viacheslav Iablokov, György Sáfrán, János Osán, István Sajó, Rafal Szukiewicz, Sergey Chenakin, Norbert Kruse: *Nanostructured MnOx as highly active catalyst for CO oxidation*, Journal of Catalysis, 287, 30–36, 2012

**chapter 3:** 2 poster presentations, 1 paper is in preparation

K. Frey, A. Beck, I. Sajó, J. Osán, G. Sáfrán, M. Veres, N. Kruse, Z. Schay: *Manganese-promoted cobalt oxide with high catalytic activity in different reactions*, 15th International Congress on Catalysis, Munich, 2012 (poster)

Beck, K. Frey, Z. Schay, L. Borkó, I. Sajó, G. Sáfrán, N. Kruse, D. Teschner: *Manganese-promoted cobalt oxide in PROX reaction*, 11th European Congress on Catalysis – EuropaCat-XI, Lyon, France, 2013 (poster)

**chapter 4:** 2 oral presentations, 1 poster

Krisztina Frey: *Catalytic activity in CO oxidation reaction over gold and silver catalysts: modelling the structure dependency*, Vienna, seminar, 2011 (oral)

Krisztina Frey, Gábor Pető, Ferenc Tanczikó, István Sajó, László Guzzi: *Role of iron oxide on gold/silver inverse model system prepared by molecular beam epitaxy*, 15th International Congress on Catalysis, Munich, 2012 (poster)

K. Frey, A. Beck, G. Pető, F. Tanczikó, I. Sajó: *Electronstructure of iron-oxid grown onto silver and silver-gold alloy catalysts by MBE*, Vienna, seminar, 2013 (oral)

**chapter 5:** 2 oral presentations, 1 poster, 1 paper is under preparation

Krisztina Frey, Tímea Benkó, Olga Geszti, László Guzzi, Zoltán Schay: *SiO<sub>2</sub> supported Ag-Au alloy nanoparticles with high catalytic activity in selective oxidation of glucose: SiO<sub>2</sub> supported Ag-Au alloy nanoparticles with high catalytic activity in selective oxidation of glucose*, International conference on Structure performance relationships in functional materials: catalysis, electrochemistry and surfactants; COST Action D36 Final Workshop, 2011 (oral)

Frey K., Benkó T., Geszti O., Schay Z. and Guzzi L.: *SiO<sub>2</sub> supported Ag-Au alloy nanoparticles with high catalytic activity in different reactions*, EuropaCat X, Glasgow, 2011 (oral)

T. Benkó, K. Frey, A. Beck, O. Geszti, L. Guzzi, Z. Schay: *Silica-supported bimetallic Ag-Au nanoparticles: Formation, structure and high activity in glucose oxidation*, 11th European Congress on Catalysis – EuropaCat-XI, Lyon, France, 2013 (poster)

We would like to use the possibility of re-evaluation of the project in two years taking into account the publications based on the project results will be appeared until that time.